LASER-PUMPED MOLECULAR LASER

B. I. Vasil'ev, A. Z. Grasyuk, A. P. Dyad'kin,
S. V. Efimovskii, A. K. Zhigalkin, Yu. I. Karev,
L. L. Losev, V. G. Smirnov, A. N. Sukhanov, and
A. B. Yastrebkov

UDC 621.373.8

The parameters of laser-pumped molecular lasers are investigated. It is established that the energy and tuning characteristics of an NH_3 laser (E_g = 1.5 J, efficiency 20%, P_{av} = 20 W, radiation frequency tuning band 753–890 cm^{-1}) are decisively influenced by the addition of N_2. A focusing raster optical-pumping system has made it possible to obtain a specific lasing energy 12 J/liter. A CF_4 laser with lasing energy 40 mJ operates in the 612–655 cm^{-1} band. Experiments on dissociation of the molecules CCl_4 and UF_6 were carried out with the aid of NH_3 and CF_4 lasers. The systems and methods of producing Raman lasers (RL) are presented. An effective RL amplifier on rotational transitions in compressed H_2, which transforms tens of beams of Nd lasers into one coherent beam of the first Stokes component with $\lambda \approx 1.13$ μm at an efficiency up to 70%, is described.

INTRODUCTION

The development of a number of scientific trends connected with selective action of laser radiation on matter, such as stimulation and control of chemical reactions [1], isotope separation [2–4], or spectroscopy of atoms and molecules [5], calls for the creation of high-power effective tunable IR lasers. Depending on the specific problem, these lasers must operate in different regimes: continuous, pulsed, or periodic-pulsed. The periodic-pulsed regime with high pulse repetition frequency is particularly important for technological applications, since it makes it possible to obtain a high average radiation power. Until recently, the only laser in the IR band satisfying all these requirements was the CO_2 laser. The tuning range of a CO_2 laser is 900...1090 cm^{-1}. However, the absorption spectra of many molecules lies in the range 500...800 cm^{-1}; therefore, the development of a high-power tunable laser in this band of frequencies is an important problem.

A promising means of producing lasers is conversion of laser radiation. Such a converter consists of two stages. The first is a laser pump source, which excites the second stage — the active medium (solid, liquid, or gas). The excitation can be resonant or nonresonant. In the case of resonant excitation, population inversion is produced in the medium. At nonresonant nonlinear optical pumping there can be no inversion.

It must be noted that the spatial separability of the pump and of the converter is the basic feature of lasers with optical pumping. It is possible to excite an active medium by several simultaneously and independently operating lasers. In this case the energy of several laser beams can be combined into one spatially coherent beam (coherent summation of laser radiation [6]). This makes it possible to increase the intensity and the specific energy output while simultaneously decreasing the beam divergence.

In the present paper we present the results of the investigations aimed at developing two basic classes of converters: with resonant and nonresonant (nonlinear-optical) laser pumping.

Translated from Trudy Ordena Lenina Fizicheskogo Instituta im. P. N. Lebedeva, Vol. 136, pp. 3-50, 1982.

0270-2010/83/0406-0537$07.50

Chapter I. MOLECULAR GAS LASERS WITH RESONANT OPTICAL PUMPING

1. Operating Principles and Basic Types of Lasers

The first converters with resonant excitation are semiconductor lasers with optical pumping [7, 8]. Subsequently, resonant pumping of liquid active media led to the development of dye lasers [9].

With the advent of high-power lasers in the IR band, molecular gases came into use as active media [10]. After the first successful experiments [10, 11] and theoretical suggestions [12], it became obvious that this class of converters is promising as a source of coherent radiation in the medium and far IR bands [13, 14].

Common to all gas lasers with optical pumping are the following: the absorption of the pump-laser radiation with excitation of vibrational–rotational levels of the molecules and production of inverted population between the levels. There exist several operating schemes of lasers with resonant optical pumping (Fig. 1). A distinguishing feature of each of them is the mechanism of excitation and the lasing mechanism. Figure 1a shows a diagram of a three-level laser,* in which the excitation and the lasing take place within the limits of one and the same vibrational band of a molecule. Level 1 pertains to the ground vibration state of the molecule v = 0, level 2 is the vibrational–rotational level of the excited state v = 1, while level 3 is the vibrational–rotational level of the excited or ground state. Upon resonant absorption of a pump photon, the molecule is excited to level 2, and in this case inversion of the populations of levels 2 and 3 can take place.

Two cases are possible here:

1) Level 3 belongs to the excited vibrational state v = 1, and its population is then very small compared with the population of level 1, since $\Delta E \gg kT$, ΔE is the energy difference between levels 1 and 3. The inverted population can be obtained at low pump intensity.

2) Level 3 pertains to the ground state v = 0, and to obtain inverted populations it is then necessary to satisfy the condition $\Delta E \gtrsim kT$. In this case the pump radiation must saturate the transition 1 → 2.

In the first case, the frequency of the laser transition 2 → 3 lies as a rule in the far IR region (wavelength 100...1000 μm); in the second, the lasing frequency differs from the pump frequency by one or two vibrational quanta (the value of the vibrational quantum is determined by the vibrational constant of the molecule B), in which case a maximum energy efficiency $\eta = h\nu_g/h\nu_p$ is obtained; this efficiency determines in final analysis the efficiency of an optically pumped laser.

At high gas pressure, population inversion and lasing can take place on many transitions. In this case the rotational sublevels of the excited vibrational state v = 1 are populated on account of rapid rotational relaxation due to collisions of the molecules. The broadening by pressure can lead to an overlap of the vibrational structure, and thus smooth tuning of the lasing frequency becomes possible.

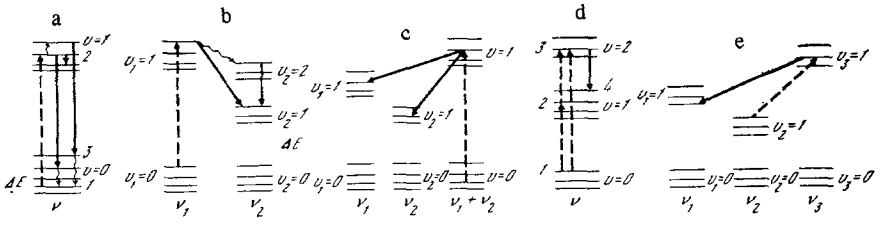

Fig. 1. Level schemes of lasers with direct optical pumping. Solid arrows — lasing; dashed — pumping.

*Population inversion in a three-level system was proposed by N. G. Basov and A. M. Prokhorov in 1956 [15].

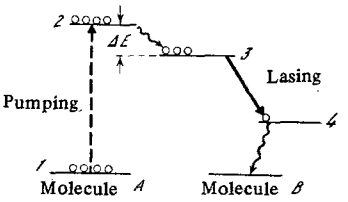

Fig. 2. Level scheme of lasers with collisional transfer of excitation to the upper laser level.

Figure 1b shows laser scheme with pumping in the ground band ν_1 and lasing in the difference band, i.e., at the transition from the level $v_1 = 1$ of the mode ν_1 to the level $v_2 = 1$ of the mode ν_2. Also possible is collisional transfer of excitation from the level $v = 1$ of mode ν_1 to the overtone $v_2 = 2$ of the mode ν_2, if the energies of these levels are close, followed by lasing in the transition from the level $v_2 = 2$ to the level $v_1 = 1$. In such schemes the lower laser level has a much lower population than that of the ground state, so that $\Delta E \gg kT$. This makes it possible to obtain a large gain and a large quantum yield.

Figure 1c shows a scheme with excitation of a compound vibration $\nu_1 + \nu_2$ and subsequent lasing in a "hot" band. One of the basic difficulties of obtaining effective lasing in this scheme is the equality of the lasing frequency to the absorption frequency of one of the component modes. Lasing is possible only when the lasing frequency lands between the peaks of the rotational structure of the absorption line. At room temperature, owing to the Doppler broadening, the rotational structure becomes smeared out, and in order for the laser to operate in accordance with this scheme it is necessary to cool the working medium and to use low pressures. This limits the gain and the efficiency of the optically pumped laser in the composite mode.

In addition to the presented schemes with single-photon excitation, laser schemes with optical excitation of overtones are also possible (Fig. 1d). The excitation can be in this case steplike or multiphoton. In steplike excitation of the level $v = 2$ it is necessary to have two pump lasers with frequencies corresponding to the transitions $1 \to 2$ and $2 \to 3$. In multiphoton excitation, the molecule absorbs from the pump field two or more photons with total energy equal to the energy of the transition $1 \to 3$, and in this case intermediate resonant levels are not necessary. Just as in the scheme 1b, the lower level 4 (the laser transition $3 \to 4$) is weakly populated, so that it is likewise possible to obtain a large gain.

Figure 1e shows a laser scheme with pumping at the difference frequency of the transition from the level $v_1 = 1$ of mode ν_1 to the level $v_2 = 2$ of mode ν_2 and with generation of a difference frequency in the transition from the level $v_2 = 1$ of mode ν_2 to the level $v_3 = 1$ of mode ν_3.

In addition to the schemes with direct optical pumping of the molecules of the same type, shown in Fig. 1, a combined scheme shown in Fig. 2 is possible. It combines optical pumping of molecules A and collisional resonant transfer of excitation from molecules A to molecules B. This method can be used to excite molecules that have no absorption line in the pumping band. This permits a considerable expansion of the range of generated frequencies of optically pumped lasers. Thus, among the main advantages of optical pumping of molecular gases are the following properties: 1) a wide band of generated frequencies and the possibility of tuning; 2) high efficiency of conversion of the pump radiation; 3) high homogeneity of the active medium after excitation, which makes it possible to obtain a laser-beam divergence close to the diffraction value.

We present below the results of an investigation of NH_3 and CF_4 lasers optically pumped by radiation of a CO_2 laser. These types of laser have by now been sufficiently well developed, have the best parameters, and have already found practical applications.

2. NH_3 Laser

The active medium is gaseous ammonia $^{14}NH_3$. The pump radiation source is a pulsed CO_2 laser. The feasibility of lasing on $^{14}NH_3$ molecules under optical resonant pumping was demonstrated in [16]. A number of subsequent studies [17–26] investigated the energy and

spectral characteristics of the lasing with both single-photon and two-step pumping [22, 23]. From among these studies notice should be taken of [19], where it was shown that addition of nitrogen as a buffer gas makes it possible to obtain lasing on many lines. In none of these investigations, however, was there achieved that combination of high energy, power, efficiency, and radiation-frequency tuning which is needed for practical applications.

The turning point in this direction was the observation by us of the decisive influence of nitrogen on the energy, power, efficiency, and tuning characteristics of the NH_3 laser [27, 28]. In [27–31] were likewise proposed and realized new optical schemes with spatially homogeneous pumping and with metallic diffraction gratings as the dispersion elements in the cavities. This has made it possible to obtain large energy and power in the pulse, and in addition, made it possible to operate in the periodic-pulse regime [31], in which high pulse and average power of the laser radiation are realized. The results obtained in [27–32] have permitted the NH_3 lasers to occupy a special place among other heretofore developed molecular lasers with optical pumping. The attained characteristics of ammonia laser are such that in the new spectral range 745–930 cm^{-1} it can be used for experiments on selective action on matter just as successfully and effectively as the CO_2 laser is used in the 930–1080 cm^{-1} band.

2.1. Spectroscopy of NH_3. The ammonia molecule has the shape of a pyramid. The nitrogen atom is located at a distance 0.38 Å from the plane in which three hydrogen atoms are located. The length of the N–H bond in the ground state is 1.02 Å. The axis passing through the nitrogen atom at equal distances from the hydrogen atoms is the principal inertia axis. The moment of inertia I about this axis, owing to the smallness of the masses of the hydrogen atoms, is small. This causes a large rotational constant of the NH_3 molecule, $B = \hbar/4\pi I$, and, consequently, an appreciable difference in energy between the neighboring rotational levels. In turn, this means a larger population difference between these levels even at room temperature, so that it is possible to obtain effective lasing at room temperature. The energy of the rotational sublevels depends on two quantum numbers J and K. J is the quantum number of the total angular momentum of the motion, and K is the projection of the momentum on the symmetry axis of the molecule. K can take on 2J + 1 values: J, J − 1, ..., −J + 1, −J. Taking into account the centrifugal perturbation in molecules of the symmetrical-top type, the expression for the energy can be represented in the form

$$W(J, K) = BJ(J+1) + (C-B)K^2 - D_J J^2 (J+1)^2 - D_{JK} J(J+1)K^2 - D_K K^4,$$

where D_J, D_{JK}, D_K are the constants of the centrifugal perturbation. Owing to the vibration of the nitrogen atom along the symmetry axis, each rotational sublevel constitutes a doublet (inversion doubling), consisting of a symmetrical (s) and antisymmetrical (a) level. The distance between the doublet components is equal to double the inversion frequency. The selection rule for the dipole transitions between vibrational levels is $\Delta J = 0, \pm 1$, $\Delta K = 0$, $s \not\rightleftarrows a$ (parallel band).

Figure 3 shows the vibrational–rotational levels of the mode ν_2 of the NH_3 molecule. The magnitude of the inversion splitting is a maximum for the ν_2 mode and increases with increasing vibrational quantum number. The R branch of the absorption spectrum of the mode $\nu_2(\Delta J = +1)$ has two lines sR(5, 0) and aR(6, 0), whose frequencies are at resonance with CO_2 laser lines 9R (30) (1084.63 cm^{-1}) and 9R(16)(1076.00 cm^{-1}), respectively. The detuning of the pump frequency from the absorption frequency amounts to $\delta\nu = 7 \times 10^{-3}$ cm^{-1} for the sR(5, 0) line and to $\delta\nu = 8 \cdot 10^{-2}$ cm^{-1} for the aR(6, 0) line. It should be noted that the width of the multiplet sR(5, k) is equal to 0.15 cm^{-1} [33] and at a CO_2-laser pump-line width 0.03 cm^{-1} particles can be captured from several levels s (5, k). When the absorbing transition in the R-branch of NH_3 is saturated, inverted population can set in with respect to the (J, K) sublevels of the excited state in $1\nu_2$ relative to the sublevel of the ground state. This corresponds to the scheme shown in Fig. 1a. Lasing develops on the P-branch transitions sP (7, 0) when pumped by the line 9R (30) and for aP (8, 0) when pumped by the line 9R (16). The lasing frequency differs from the pump frequency by an amount equal to two rotational quanta ($\sim$250–300 cm^{-1}). The thermal population of the end point laser

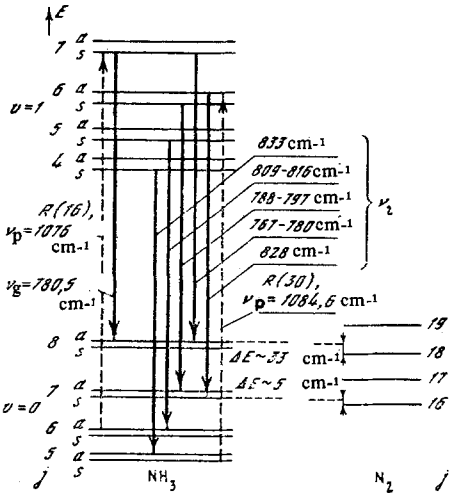

Fig. 3. Scheme of part of the vibrational–rotational levels of the mode ν_2 of the $^{14}NH_3$ molecules and of the rotational sublevels of the nitrogen molecule. Solid arrows — lasing; dashed — pumping.

levels is ∿25% of the population of the level from which the pumping takes place, so that saturation of the absorption is necessary. It is possible to extend substantially the range of generated frequencies by adding to NH_3 a buffer gas. The rapid rotational relaxation in collisions with the molecules of the buffer gas leads to population inversion on many sublevels of the $1\nu_2$ level [34] and consequently to the possibility of lasing on many frequencies. In addition, as shown in [28], the fact that the buffer gas has levels that are at resonance with the lower levels of the laser transitions leads to a considerable increase of the lasing energy and of the laser efficiency.

2.2. Optical Schemes of NH_3 Lasers. Figures 4–7 show different optical schemes of NH_3 lasers. In [27] there was employed for the first time a longitudinal variant of optical pumping with an unfocused beam. This has made it possible to obtain spatially homogeneous excitation of a large volume of working laser medium. The scheme presented in [27] (Fig. 4) suffers from the shortcoming that in the cavity of the NH_3 laser is located the cell of a CO_2 laser, which introduces substantial active losses, thereby considerably deteriorating the parameters of the lasing. The use of a scheme with separated cavities, described in [30] (Fig. 5), has made it possible to avoid this shortcoming. The scheme of the tunable NH_3 laser is shown in Fig. 6 [32]. The CO_2-laser emission from the zeroth order of the grating G_1 (100 lines/mm, blaze angle 30°) was incident in a direction close to the normal of the grating G_2 (75 lines/mm, blaze angle 23°), and was fed into the cell with NH_3 via the first order of the latter (for the pump frequency). The NH_3-laser cavity was made up of mirror M_2 (with radius R = 10 m) and grating G_3 (100 lines/mm, blaze angle 30°), which were coupled through the zeroth order of the grating G_2. The lasing radiation was extracted via the first order into two channels: the first channel in the case of incidence from the side of the grating G_3, and the second for incidence from the side of the mirror M_2. The second channel contained 40% of the energy in the first. Tuning of the NH_3-laser generation frequency was effected by rotating the grating G_3. The laser cell with NaCl windows inclined at the Brewster angle was made of stainless steel, and had a length 180 cm and an inside diameter 67 mm. The absence of optical elements with low optical strength in the cavity (prisms, selective mirrors, etc.) made it possible to use the scheme described in the periodic-pulse regime at a high average pump power (up to 1 kW) [31].

An essential characteristic of gas lasers is the specific heat output. An increase of the energy picked off per unit volume of the active medium is connected with an increase in the density of the spatially homogeneous pumping. It is known that the maximum effect is produced by a combination of a light pipe with pumping through a raster focusing system. In this case it is possible to combine most fully the requirement of homogeneity and intensity of the pumping. In [29] was investigated an ammonia laser with a raster optical-pumping

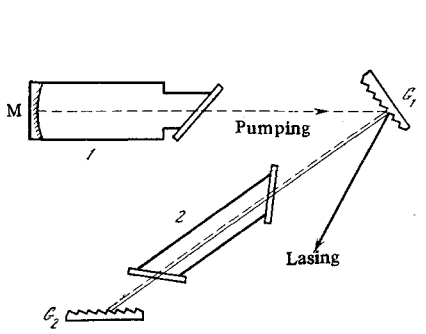

Fig. 4

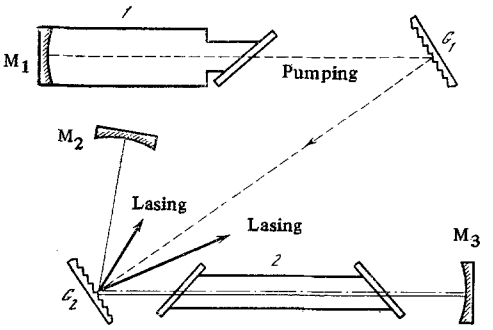

Fig. 5

Fig. 4. Optical scheme of ammonia laser with common cavity: 1) CO_2 laser; 2) NH_3 laser.

Fig. 5. Optical scheme of ammonia laser with nonselective cavity: 1) CO_2 laser; 2) NH_3 laser.

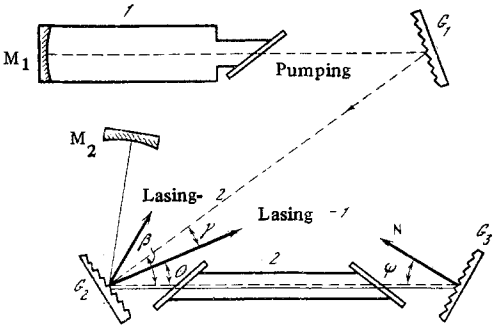

Fig. 6. Optical scheme of ammonia laser with selective cavity: 1) CO_2 laser; 2) NH_3 laser.

system. The experimental setup is shown in Fig. 7. The pump radiation was focused into a light pipe 70 cm long, placed in a glass cell with the aid of a short-focus raster system (F = 25 cm, cross section of the beam at the focus 7 × 7 mm). The raster, made of BaF_2, constituted two crossed sets of wedges, which formed cylindrical surfaces. The spot obtained at the focus of the raster system had a square cross section equal to the dimension of the raster mesh. The pump energy passing through the raster system decreased to 3.5–4 J. The cell windows were made of NaCl and were oriented at the Brewster angle. The light pipes were assembled copper waveguides of quadratic cross section (5 × 5 and 10 × 10 mm). The cavity of the NH_3 laser consisted of a total-reflection mirror M_1 (15 mm diameter) and a flat semi-transparent plate M_2 (NaCl, Si, ZnSe). The laser emission ($\nu_g \sim 800$ cm^{-1}) was directed to a calorimeter. The diverging pump background radiation was cut off with a diaphragm.

The radiation energy was measured with calorimeters KIM-1 and VChD-1. The temporal characteristics of the pump radiation and of the lasing radiation were investigated with FPU-50 and FPU-250 photoreceivers in which the electrons are dragged by photons [35, 36], and an S8-2 oscilloscope. The lasing frequencies were measured with an IKM-1 monochromator, in which the Litrow mirror was replaced by a diffraction grating of 100 lines/mm, thus ensuring a resolution not worse than 0.5 cm^{-1}.

2.3. Characteristics of NH_3 Lasers. a. *Single-pulse regime.* In our experiments the NH_3 laser was pumped by the lines 9R(16) and 9R(30) of the 9-μm lasing region of the CO_2 laser. The pump transitions correspond to the designations αR(6,0) and sR(5,0), and the lasing transitions to αP(8,0) and sP(7,0) (lasing frequencies 780 and 828 cm^{-1}, respectively).

As shown in [28], addition of nitrogen to the NH_3 makes it possible to raise substantially the lasing energy and the efficiency of the NH_3 laser, and in the case of pumping by the 9R(30) line the energy increases by one order of magnitude, whereas when pumping by the 9R(16) line it increases by 2–3 times. An investigation of the influence of He and H_2 used as buffers when pumping with the 9R(30) line has shown that in these cases the energy was approximately

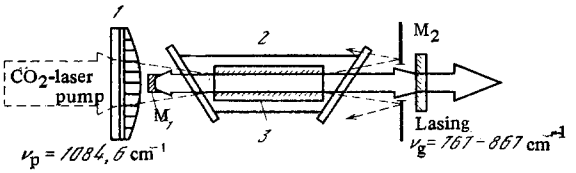

Fig. 7. Optical system of light-pipe ammonia laser with raster pump system: 1) raster; 2) NH_3 laser; 3) light pipe.

TABLE 1

ν, cm^{-1}	Transition	E_g, mJ	ν, cm^{-1}	Transition	E_g, mJ
881,1	*sP* (4, K)	400	814,3	*aP* (6,3)	600
872,6	*aP* (3,1)	550	812,0	*aP* (6,4)	450
	aP (3,2)				
			809,7	*aP* (6,5)	400
868,0	*P* (5,K)	900	798,0	*aP* (7,1)	500
853,6	*aP* (4,0)	1000	797,4	*aP* (7,2)	500
	aP (4,1)		796,0	*aP* (7,3)	500
852,2	*aP* (4,2)	950	794,0	*aP* (7,4)	250
851,0	*aP* (4,3)	800	791,8	*aP* (7,5)	320
847,4	*sP* (6,K)	800	789,0	*aP* (7,6)	450
834,7	*aP* (5,1)	650		*aP* (8,0)	350
834,0	*aP* (5,2)	800	780,4	*aP* (8,1)	
832,0	*aP* (5,3)	870	779,4	*aP* (8,2)	350
830,2	*aP* (5,4)	640	778,2	*aP* (8,3)	250
828,0	*sP* (7, K)	880	776,4	*aP* (8,4)	200
816,8	*aP* (6,0)	920	774,0	*aP* (8,5)	200
816,2	*aP* (6,1)		770,9	*aP* (8,6)	350
815,4	*aP* (6,2)	860	749,8	*aP* (9,7)	200
			745,3	*aP* (9,8)	200

doubled. Such a strong influence of nitrogen on the lasing energy when pumping with the 9R(30) line is explained by the fact that N_2 has levels that are quasiresonant with the end-point laser levels [28] (Fig. 8), and the collisions of NH_3 with N_2 lead to rapid depopulation of these levels. The absence of a similar effect when the 9R(16) line is used for the pumping is attributed to the strong detuning of the pump frequency from the absorption ($\Delta\nu \sim 0.08$ cm^{-1}). Figure 9 shows the dependences of the energy E_g of lasing on the 828 cm^{-1} line (transition sR(7, 0)) for different compositions of the mixtures NH_3:N_2 on the total pressure p_Σ of the mixture. For the optimal mixture NH_3:N_2 = 1:75 at a pressure p_Σ = 60 torr the lasing energy in the first and second channel amounted to $\approx$1.3 J at an efficiency $\approx$20% relative to the total energy. The use of high pressure of the mixture of the gases NH_3 and N_2 lowered considerably the time of rotational relaxation and made it possible to retune the NH_3 frequency when pumping with the 9R(30) line. Figure 10 shows the spectral-energy characteristic of an NH_3 laser. It can be seen that the spectrum consists of groups of lines, and this corresponds to (J, K) transitions.

Table 1 shows the identification of the characteristics of the lasing spectral lines. The maximum energy was $\sim$1.5 J at an efficiency $\sim$21% and a frequency 853 cm^{-1}. Comparison with Fig. 8 shows a complete correlation of the distribution with respect to energy on Fig. 10 with the pressure of resonances of lower laser levels with rotational levels of nitrogen, thus confirming the role of nitrogen as a "refrigerator" for many laser levels. For the lasing frequency 781 cm^{-1}, the energy obtained was $\sim$400 mJ, which was much higher and more effective than lasing at the same frequency when pumped by the 9R(16) line. All the subsequent results were obtained only for an NH_3 laser pumped by the 9R(30) line. For the most intense lines we plotted the lasing energy against the mixture composition and the total pressure. The measurements have shown that for all these lines the optimal are the mixtures NH_3:N_2 = 1:75...1:100 and the optimal total pressure is $p_\Sigma \sim 60$ mm torr.

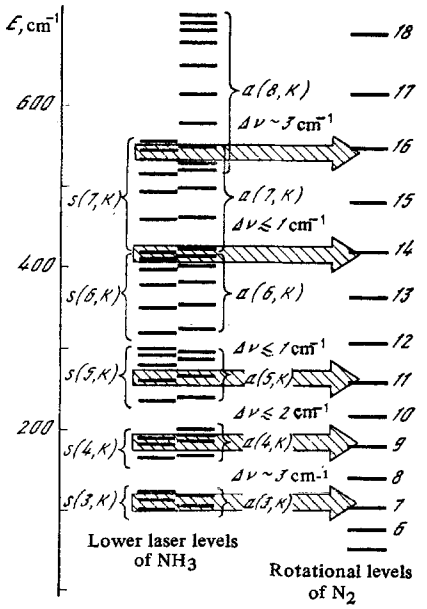

Fig. 8. Scheme of lower laser levels of the NH_3 molecules and of the rotational levels of nitrogen.

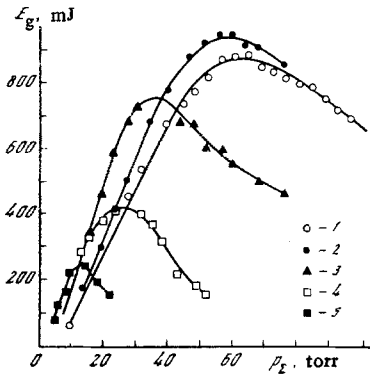

Fig. 9

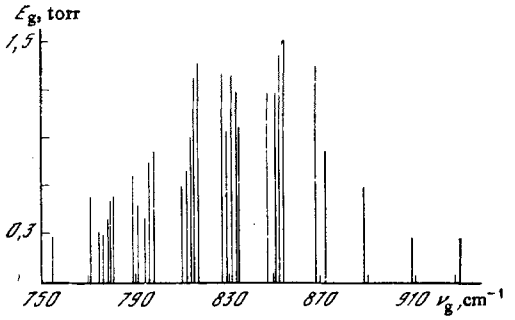

Fig. 10

Fig. 9. Dependences of the NH_3 laser generation energy on the total mixture pressure NH_3:N_2 (for different mixtures): 1) 1:100; 2) 1:75; 3) 1:50; 4) 1:25; 5) 1:10. Pumping by means of the 9R(30) line.

Fig. 10. Lasing spectrum of ammonia laser.

To optimize the parameters of the NH_3 laser and to determine ways of increasing the efficiency, the physical mechanisms of the pumping and lasing were investigated. Figure 11 shows oscillograms of the lasing pulses at the frequency $\nu_1 = 828$ cm^{-1} at various pressures of mixture NH_3:N_2 = 1:100 (a, b, c). Also shown are oscillograms of the pump pulse at the entrance (d) and at the exit (e–h) from the active medium in the ammonia-laser generation regime. Since the intensity at the pump peak is much larger than the intensity at the tail, the peak and the tail of the pump pulse will be differently absorbed. The nonlinear absorption coefficient is given by the relation

$$\alpha = \frac{\alpha_0}{1 + I/I_s}, \qquad (1)$$

where α_0 is the linear absorption coefficient and I_s the saturation intensity.

At $I \ll I_s$ we have $\alpha \sim \alpha_0$ and at $I \gg I_s$ we have $\alpha \ll \alpha_0$. If the saturation intensity I_s is reached at the peak of the pump pulse, then, inasmuch as lasing calls for satisfaction

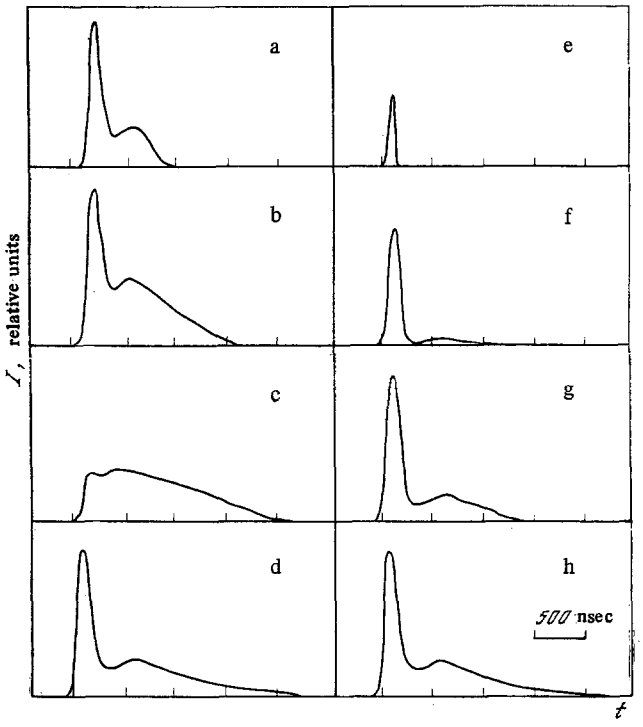

Fig. 11. Oscillograms of pump and lasing pulses: *a*, b, c) lasing (ν_g = 828 cm^{-1}); d) pump radiation at the entrance to the cell; e–h) pump radiation at the exit from the cell; pressure p_Σ of mixture NH_3: N_2 = 1:100: *a*) 100; b) 60; c) 30; e) 70; f) 30; g) 10; h) 0 torr. [Pressure d) is not indicated in original Russian caption – Publisher.]

of the condition $I \sim I_g$, the lasing-pulse duration will be less than the total duration of the CO_2 pumping pulse. With decreasing I_s the lasing pulse duration should increase. The saturation intensity is given by

$$I_s = h\nu/2\sigma T_1, \tag{2}$$

where $h\nu$ is the energy of the absorption quantum, σ is the absorption cross section, and T_1 is the longitudinal-relaxation time. In our case $T_1 \sim \tau_{V-T}$ is the time of the vibrational–translational relaxation. The pump absorption cross section is

$$\sigma = \frac{g(\nu)}{8\pi\tau_{sp}}\cdot\frac{\nu^2}{c^2}, \tag{3}$$

τ_{sp} is the spontaneous lifetime of the upper level, $g(\nu)$ is the form factor of the line. In the ammonia pressure region >1.5 mm torr, the collisional half-width of the absorption line exceeds the Doppler half-width, which is given for ammonia at room temperature by

$$\Delta\nu_D = 1.5\cdot 10^{-6}\nu. \tag{4}$$

In the case of collisional broadening the line contour is Lorentzian

$$g(\nu) = \frac{1}{\pi}\frac{\Delta\nu}{(\nu-\nu_0)^2+(\Delta\nu)^2}, \tag{5}$$

where $(\nu - \nu_0)$ is the deviation of the pump frequency from absorption, and $\Delta\nu$ is the collisional half-width. The coefficients of broadening by pressure are equal to [33]: K_{NH_3} = 28

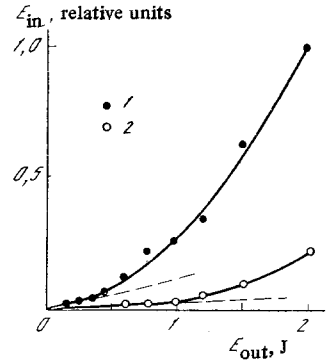

Fig. 12

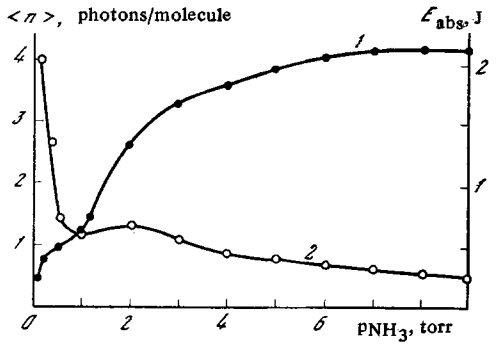

Fig. 13

Fig. 12. Dependence of the CO_2 laser emission energy at the exit from the cell with NH_3 on the energy at the entrance to the cell: 1) 2 torr; 2) 4 torr.

Fig. 13. Dependence of the absorbed radiation energy (1) of a CO_2 laser and of the number of absorbed photons by one molecule (2) on the ammonia pressure (E_{1N} = 2 J).

MHz/torr — the self-broadening coefficient; K_{N_2} = 3.8 MHz/torr — the coefficient of broadening by nitrogen. It follows therefore that for NH_3:N_2 mixtures we have $\Delta\nu \sim (p_{NH_3} + 0.14\, p_{N_2})$. The saturation intensity I_s, as follows from the formula presented above, is proportional at high mixture pressures to p_{Σ}^2 ($\Delta\nu >> \nu - \nu_0$); thus, by varying the pressure (and by the same token I_s) it is possible to vary the duration of the lasing pulse.

At an intensity $I << I_s$ at the peak, the entire pulse is linearly absorbed. With increasing pulse intensity, when I_s is reached in the peak, nonlinear absorption sets in. Figure 12 shows the dependence of the output energy E_{out} on the input energy E_{in} for different ammonia pressures. It can be seen that for high pressure the deviation from linearity of the absorption sets in at high intensity, corresponding to larger I_s. At a known temporal pump-pulse waveform, the following empirical formula was obtained for the saturation intensity:

$$I_s = (0.025p^2 + 1.2) \text{ MW/cm}^2, \tag{6}$$

where p is the ammonia pressure, torr.

Knowing I_s, we can estimate the longitudinal-relaxation time T_1 NH_3-NH_3, and also the cross section σ for the pump-radiation absorption. When the pump beam passes through an absorbing layer of length L, its intensities at the input and at the output satisfy the equation

$$\ln \frac{I_{in}}{I_{out}} + \frac{I_{in} - I_{out}}{I_s} - \alpha_0 L = 0, \tag{7}$$

where α_0 is the coefficient of linear absorption. The energy absorbed in the layer is given by

$$E_{abs} = \int_0^{\tau_{pul}} (I_{in} - I_{out})\, dt. \tag{8}$$

At high pressure (the detuning is much less than the impact broadening), α_0, and with it also $E_{abs} = E_{in}\,(1 - \exp[-\alpha_0 L])$, does not depend on p, i.e., E_{abs} should reach a plateau with increasing pressure. Figure 13 shows the dependence of the absorbed energy in pure ammonia and of the number of absorbed photons by one molecule <n> on the gas pressure p_{NH_3}. The value of α_0 determined from this relation turned out to be 0.05 $cm^{-1} \cdot torr^{-1}$, and the cross

section for the absorption of the pump radiation on the transition SR(5, 0) is $\sigma \simeq 1.5 \cdot 10^{-16}$ cm^2. The time of longitudinal relaxation $T_{1\ NH_3\text{-}NH_3}$, estimated from the saturation intensity and the absorption cross section, turned out to be (450 ± 50) nsec·torr. It should be noted that the "slope" of the approach of the plot shown in Fig. 3 to the plateau of E_{abs} as a function of p_{NH_3} depends substantially on $T_{1\ NH_3\text{-}N_2}$. The dependence of the absorbed energy on the pressure was calculated for the pump pulse whose shape is shown in Fig. 11. The calculation was carried out in the following manner. The time variation of the pump pulse was tabulated. For each value of the intensity the transcendental equation (7) for I_{out} was solved at different pressures of NH_3, after which the value of E_{abs} was obtained from (8). The ammonia pressure determines the absorption cross section (σ), and the V—T relaxation time $T_{1\ NH_3\text{-}NH_3} = T_1^\circ \cdot p^{-1}_{NH_3} \cdot T_1^\circ$ was varied in a wide range. The calculated relations have shown good agreement with the experimental curve at $T_1^\circ \sim 500$ nsec·torr. Similar measurements were made for the NH_3:N_2 mixture. The results of these measurements are shown in Fig. 14. The relaxation time $T_{1\ NH_3\text{-}NH_3}$ of ammonia in a nitrogen medium, determined from these relations, turns out to be (2.5 ± 0.5) μsec·torr.

One of the mechanisms that limit the pump intensity is excitation of high vibrational levels, which leads to a decrease of the inversion on the working transition, i.e., to a decrease of the NH_3-laser efficiency. Figure 14 shows the dependence of the number of absorbed photons per molecule on p_Σ. It can be seen that at low pressures the multiphoton excitation plays an essential role. With increasing pressure, the number of photons per molecule decreases and this is apparently due to the increase of the role of the (V—V') exchange.

A similar dependence was plotted in the lasing regime at the frequency $\nu_g = 828$ cm^{-1}. The results are shown in Fig. 15. The plot of the absorbed photons per molecule differs from the plot obtained without lasing. The reason is that in the lasing regime the NH_3 molecules are rapidly dropped from the upper laser level $a(6, 0)$ to the lower level s(7, 0). After relaxation on the s(5, 0) level, from which the pumping takes place, the molecules can participate several times during the time of action of the pump pulse in the process consisting of pumping → relaxation → lasing → relaxation → pumping → ... .

The dashed line in Fig. 15 shows the dependence of the cross section for the pump-radiation absorption on the mixture pressure. It can be seen that the number of absorbed photons per molecule duplicates the variation of the cross section; this indicates that the main contribution to the absorption is made by excitation of the transition sR(5,0). It can thus be concluded that the lasing regime is quasistationary. It must be noted that a significant role can be played by exchange processes as well as by multistep excitation. The obtained quantum efficiency amounted to 40%, possibly due to these processes. A more detailed study of the processes V—V' and V—V and of the multistep excitation is the subject of further research.

The investigations performed show that to increase the efficiency of an NH_3 laser it is necessary to optimize the pump waveform, i.e., its intensity and duration. Figure 16 shows the temporal characteristics of the lasing pulses for different pump pulses. The pump energy is the same. It can be seen that pumping by a long pulse (a) of lower intensity makes for a higher conversion efficiency than pumping by a short pulse (b) of high intensity, inasmuch as the part of the pump pulse with $I > I_s$ is not used. Consequently, the optimal pulse for pumping is of intensity $I \sim I_s$. The pulse duration is limited by the heating of the gas, and this leads to an increase of the thermal population of the lower laser levels.

As already noted above, the use of a raster focusing system in conjunction with a light pipe makes it possible to increase the pump density and increase the energy output from a liter of working medium of an NH_3 laser.

An investigation of the influence of the cavity Q on the lasing energy has shown that at a given cavity geometry the maximum lasing energy is obtained if the initial mirror used

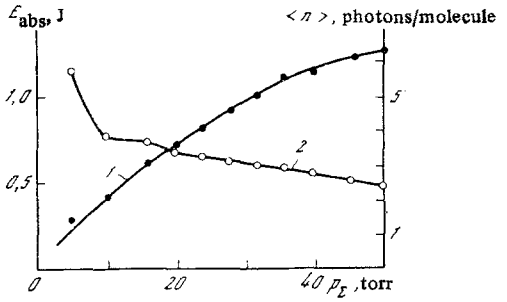

Fig. 14

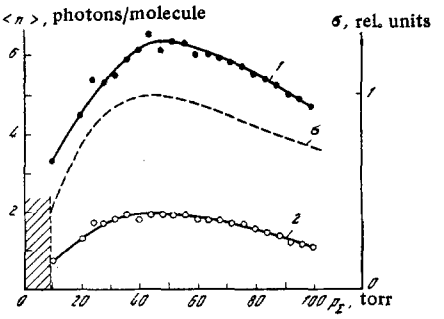

Fig. 15

Fig. 14. Dependence of the energy (1) of the CO_2 laser radiation absorbed in a $NH_3:N_2$ = 1:50 mixture on the mixture pressure, and dependence of the number of absorbed photons per NH_3 molecule (2) in the absence of lasing.

Fig. 15. Average number of photons absorbed (1) and emitted (2) by one NH_3 molecule in the $NH_3:N_2$ = 1:50 mixture in lasing at ν_g = 828 cm^{-1} vs the mixture pressure. The shaded region corresponds to the condition $\Delta\nu_D \gtrsim \Delta\nu$.

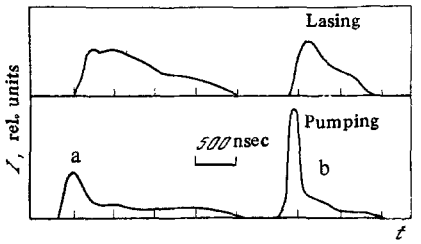

Fig. 16. Oscillograms of the lasing pulses of NH_3 laser pumped by long (*a*) and short (b) CO_2 laser pulses at identical energy in the pump pulse; E_p^n = 0.5 J·cm^{-2}; p_Σ = 20 torr; mixture $NH_3:N_2$ = 1:50.

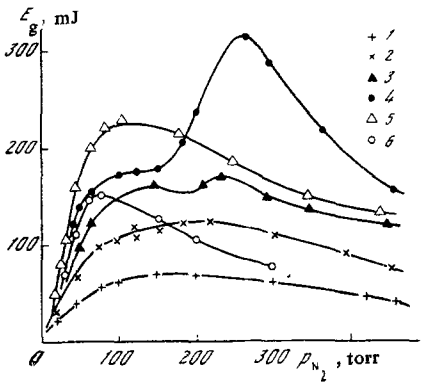

Fig. 17

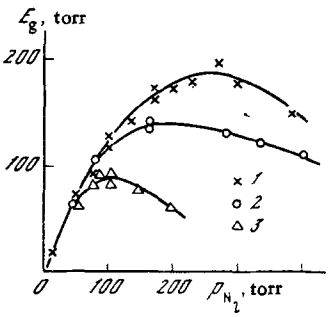

Fig. 18

Fig. 17. Dependence of the generation energy of an ammonia laser with a raster system using a light pipe of 10 × 10 mm cross section on the pressure of the N_2 at the following values of p_{NH_3}: 1) 0.5 torr; 2) 0.7; 3) 0.9; 4) 1.2; 5) 1.4; 6) 1.6 torr.

Fig. 18. Dependence of the lasing energy (E_p = 3.5 J) of an ammonia laser with a raster system using a light pipe of cross section 5 × 5 mm on N_2 pressure at the following values of p_{NH_3}: 1) 1.8; 2) 1.5; 3) 2.5 mm torr.

TABLE 2

Light pipe		Optimal comp. of mixture		Energy, J	Efficiency, %	Specific energy output, J/liter
length, cm	cross section cm^2	$NH_3 : N_2$	total pressure, torr			
70	1×1	1 : 200	230	0,35	10	5
70	0,5×0,5	1 : 150	280	0,2	6	12

is a ZnSe plate (with a reflection coefficient ∿36%). The dependence of the lasing energy on the buffer-gas pressure p_{N_2} at different values of p_{NH_2} for a ZnSe output mirror are shown in Figs. 17, 18. Figure 17 shows the pressure dependence of the energy of an NH_3 laser with a copper light pipe of cross section 10 × 10 mm at various parameters p_{NH_2}. The maximum lasing energy (0.35 J) was obtained at an ammonia pressure p_{NH_3} = 1.2 mm torr and at a nitrogen pressure p_{N_2} = 200 mm torr. Figure 18 shows a similar dependence for a light pipe with cross section 5 × 5 mm. In this case the maximum lasing energy was 0.2 J at pressures p_{NH_2} = 1.8 mm torr and p_{N_2} = 270 mm torr. The shift of the lasing maximum toward higher ammonia pressure is due to the increase of the pump density E^n from 4 to 16 J/cm^2. In the former case the specific energy output was 5 J/liter, and in the latter 12 J/liter, values comparable in order of magnitude with the specific energy of a CO_2 laser. The decrease of the efficiency from 10% for a 10 × 10 light pipe to 6% for a 5 × 5 light pipe is due to diffraction losses of the cavity (the Fresnel number is $N = a^2/L\lambda \simeq 1.5$).

It is interesting to note that a high specific energy output was obtained at a low pressure of the active particles (1–2 torr). The high pressure of the N_2 buffer gas (∿300 torr), which noticeably decreases the time of the rotational relaxation, can ensure participation of all the NH_3 molecules in the lasing process. But even in this case, as shown by estimates, during the time of the pump pulse each ammonia molecule manages to reradiate an infrared photon 10 and more times.

For the 10 × 10 light pipe we measured the NH_3 laser beam divergence, which amounted to 4×10^{-3} rad, a value close to the diffraction limit.

It is seen from Fig. 17 that lasing was maintained up to a buffer-gas (N_2) pressure 400... 500 mm torr. Consequently, it is possible to use as a buffer gas air, whose main component is nitrogen. Lasing was obtained on a mixture of ammonia and ordinary air with total pressure 1 atm. The maximum lasing energy was 20 mJ.

These results reveal the possibility of developing an atmospheric laser with a forced flow of ammonia through the light pipe or with a stationary mixture of ammonia with air, so as to eliminate from the optical system elements with low radiation endurance (NaCl windows). Experiments of this type were performed. The lasing energy amounted to 2 mJ. So low an energy is due apparently to the diffusion of the ammonia molecules from the pumping zone. Pumping in accordance with the system shown in Fig. 7 can be effected by several simultaneously and independently operating CO_2 lasers. In this case the NH_3 laser will operate in the regime wherein the energies of several incoherent sources are summed to form a single spatially coherent beam [6]. The basic parameters of an NH_3 laser with a raster system for optical pumping, ν_g = 852–816 cm^{-1} (pump source CO_2 laser, R(30), ν = 1084.6 cm^{-1}, E_p = 3.5 J), are listed in Table 2. Thus, the employed raster scheme has made it possible to increase by more than one order of magnitude the specific energy output of the NH_3 laser with optical pumping at high efficiency (up to 10%). In addition, the investigations uncover the possibility of developing an effective atmospheric laser using ammonia molecules and having high power.

b. *Periodically pulsed regime.* From the point of view of using infrared lasers in technological processes, an important characteristic, besides the energy in the pulse, is the

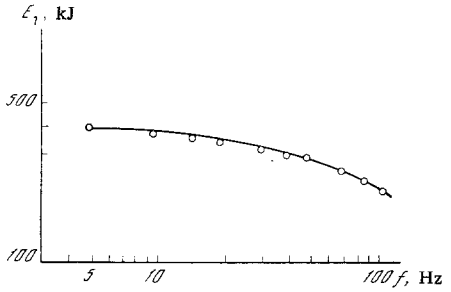

Fig. 19

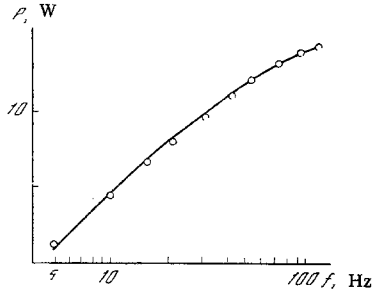

Fig. 20

Fig. 19. Dependence of the lasing energy per pulse of an NH_3 laser on the pulse repetition frequency when working in the periodic-pulse regime. Pumping by the 9R(30) line; ν_p = 1084.6 cm^{-1}; $NH_3:N_2$ = 1:50, p_Σ = 20 torr.

Fig. 20. Dependence of the average lasing power of an NH_3 laser on the pulse repetition frequency. Pumping by the 9R(30) line; ν_p = 1084.6 cm; $NH_3:N_3$ = 1:50, p_Σ = 20 torr.

average radiation power, which determines in final analysis the productivity of the method. Therefore, an increase of the average power of an NH_3 laser operating in the periodic-pulsed regime is of great interest for isotope separation and for laser chemistry. In [31] is described an NH_3 laser operating in the periodic-pulse regime with a pulse repetition frequency f up to 100 Hz. Lasing was obtained by pumping NH_3 in a nonselective cavity by radiation from a CO_2 laser with high pulse repetition frequency. Owing to the nonselectivity of the cavity, when pumping a $NH_3:N_2$ mixture on the 9R(30) line there were registered in the lasing spectrum six lines, the four more intense of which had frequencies 833, 828, 800, and 781 cm^{-1}. The energy in these lines amounted to 30, 60, 7, and 2% of the total energy, respectively. It should be noted that all the presented results on the energy and average power when pumping an $NH_3:N_3$ mixture represent the total lasing energy on the indicated lines. The pump energy on the R(30) line amounted in this case to 2.5 J. We used a nonoptimal $NH_3:N_2$ = 1:50 mixture. The efficiency obtained in this manner was approximately 16%. The dependences of the energy and the average power on the pulse repetition frequency were investigated. Figure 19 shows the dependence of the lasing energy in the pulse on the pulse repetition frequency when pumped on the R(30) line.

It can be seen from Fig. 19 that with increasing frequency the energy in the pulse decreases, owing to heating of the working medium. Heating leads, first, to a decrease of the particle density within the confines of the pump beam; second, it leads to an increase of the thermal population of the lower laser levels. Both effects decrease the lasing energy in the pulse. However, despite the decrease of the pulse energy, the average lasing power of the NH_3 laser increases with increasing pulse repetition frequency, up to 100 Hz. The maximum average power P reached a value 20 W. It can be seen from Fig. 20 that with increasing pulse repetition frequency to >100 Hz it is possible to increase the average power still more. The obtained average lasing power in the 12-μm region is comparable with the power of ordinary CO_2 periodic-pulse lasers. The use of a selective cavity (see Fig. 6) makes it possible to obtain a periodic-pulse regime on many lines in the range 745–930 cm^{-1}. The combination of high pulse power and average radiation power in this band makes it possible to use the NH_3 laser for a large number of applications.

2.4. Discussion of Results and Conclusions. Addition of nitrogen to ammonia has made it possible to increase the efficiency of the NH_3 laser to 20%. However, this high efficiency is still not the limit. One can hope that optimization of the pump-pulse waveform with respect to intensity and with respect to duration, and also optimization of the length of the active region, will make it possible to increase the efficiency substantially, up to the maximum possible (70%), determined by the ratio ν_g/ν_p.

The increase of the pump density with the aid of a raster + light-pipe system by summation of pulses makes it possible to operate at a buffer gas pressure ∿1 atm and higher. At such high pressures, the overlap of the rotational–vibrational levels on account of collisional broadening can lead to a smooth tuning of the lasing frequency. In addition,

population of the sublevels of the overtone $2\nu_2$ becomes possible on account of rotational and (V–V) relaxation, inasmuch as already at J = 8 the levels (J, K) of the first-excited state $1\nu_2$ have the same energy as the lower levels $2\nu_2$, e.g., the energy of the $1\nu_2$ level $a(8, 0)$ is 1676.67 cm^{-1}, while that of the $2\nu_2$ level s(1, 0) is 1617.84 cm^{-1}. It is thus possible to extend the tuning range of the NH_3 laser into the region >14 μm. It is as yet impossible to draw any definite conclusion concerning the direct excitation of higher vibrational states at pump densities >2 J/cm^2.

As follows from Eq. (5), when the nitrogen pressure is increased the absorption coefficient α_0 is decreased. The result is that the intensity is more uniformly distributed over the length of the cell than in the case of large α_0. Consequently, it is possible to pump a large volume of active medium in conjunction with a large specific energy output at a high pump density. This will make it possible in the future to raise the energy parameters of the NH_3 laser to the level of modern CO_2 lasers. At the present time, as can be seen from our study, we have a small energy output ∿1 J/liter at a high efficiency (20%), and a high energy output in a raster system at a lower efficiency (10%). The problem is to increase the efficiency and maintain the high energy output. The divergence of an NH_3 laser can be substantially lower than that of CO_2 lasers, since the active medium of the CO_2 laser is highly inhomogeneous, owing to perturbations in the electric discharge. The divergence measured in our experiments was 4×10^{-3} rad, which is close to the diffraction limit.

It has also been shown that it is possible to achieve the desired waveform of the pulse and control its duration. The results of the investigation of the characteristics in the periodic-pulse regime and when pumped by long pulses gives grounds for hoping to realize a continuous operation of the NH_3 laser. The problem of heating of the working medium in the pump channel can be solved by organizing in a suitable manner the gas flow, as is done at the present time in a CO_2 laser with high pulse repetition frequency.

The investigations performed offer evidence that the NH_3 laser is highly promising for a number of applications, especially for selective action on matter. Its high efficiency, energy, pulsed power, and also operation in the periodic-pulsed regime with high average power make the NH_3 laser comparable with the CO_2 laser, i.e., at the present time the (9–13)-μm band can be regarded as covered by laser radiation with the parameters need for technological processes such as laser isotope separation.

3. CF_4 Laser

The possibility of lasing on the CF_4 molecules pumped by a CO_2 laser was demonstrated in [37]. In the succeeding studies [38, 28, 39] the energy and temporal characteristics were investigated, as well as the possibility of tuning near 16 μm [28, 39]. A detailed investigation of the spectroscopy of the CF_4 molecule and of the tuning characteristics of the CF_4 laser is given in [40].

3.1. Absorption of Pump Radiation by CF_4 Molecule. For optical pumping of the CF_4 molecule one uses absorption at the composite frequency $\nu_2 + \nu_4$ (Fig. 21). This absorption is sufficiently noticeable only in the region of the R(12) line of the CO_2 laser (1073.3 cm^{-1}). Measurements of the absorption coefficient on this line under our conditions at T = 300°K yielded $\alpha = 1.3 \cdot 10^{-4}$ $cm^{-1} \cdot torr^{-1}$, which is close to the value $1.1 \cdot 10^{-4}$ $cm^{-1} \cdot torr^{-1}$ in [37]. At T = 150°K the absorption coefficient increases to $2.5 \cdot 10^{-4}$ $cm^{-1} \cdot torr^{-1}$. These values, however, were obtained under conditions of saturation of the transition. The determination of the linear absorption coefficient and of the saturation parameter calls for a more detailed investigation.

The dependence of the absorption coefficient on the pressure at a pump density 2 J/cm^2 (the line R(12)) was investigated at an absorbing-layer length 165 cm. In the pressure range 1–50 torr, the absorption coefficient is constant and is equal to $1.3 \cdot 10^{-4}$ $cm^{-1} \cdot torr^{-1}$. This behavior shows that only one rotational line takes part in the absorption. The rotational constant for the CF_4 molecule is B = 0.1919 cm^{-1}, and the vibrational angular momentum constant is $\zeta_4 = -0.36$, so that the spacing of the individual absorption lines in the band is $\nu_2 + \nu_4$ $2B(1-\zeta_4) = 0.52$ cm^{-1}. For a typical collisional-broadening constant of the rotational lines 30 MHz/torr, the broadening at p = 50 torr does not exceed 0.05 cm^{-1}. The field broadening of the absorption line at intensities 10–20 MW/cm^2 is also small, because of the smallness of the dipole moment of the transition at the composite frequency. Therefore, no other rotational lines become involved under our conditions.

Absorption of the pump energy at the frequency 1073.3 cm^{-1}, as a function of the input energy, was investigated at CF_4 pressures 1, 4.4, and 10 torr. The length of the absorbing

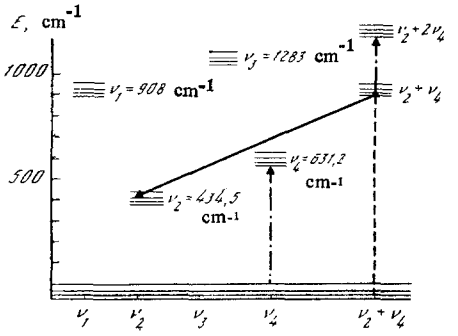

Fig. 21

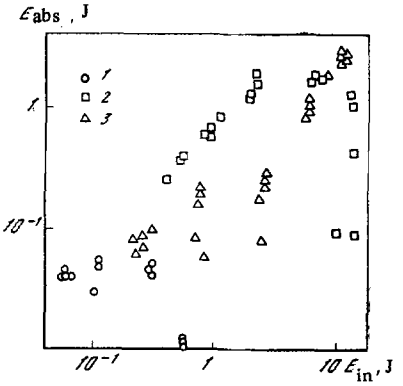

Fig. 22

Fig. 21. Level schemes of optically pumped laser operating on CF_4 molecules. Solid lines — lasing; dashed — pumping; dash-dot — absorption.

Fig. 22. Dependence of the energy absorbed in CF_4 gas on the input energy at gas pressures: 1) 1; 2) 4.4; 3) 10 mm torr.

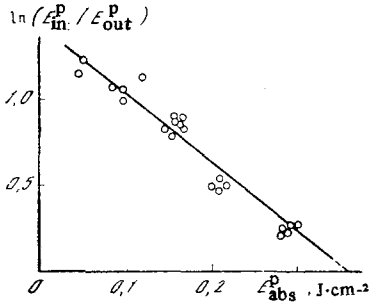

Fig. 23. Dependence of the logarithm of the ratio of the densities of the incident and transmitted energies on the density of the absorbed radiation energy of a CO_2 laser (line 9R(12)).

layer in the first case was 400 cm, and in the last two cases 165 cm. The dependence of the energy absorbed in the gas as function of the incident energy is shown in Fig. 22. It can be seen that with increasing input energy the absorbed energy at a given pressure first increases, then reaches saturation, with the exception of p = 1 torr, where the saturation is observed at the lowest employed pump energy levels. At the absorption maximum, the energy per CF_4 molecule is $\sim$0.5 photon at p = 4.4 and 10 torr, and $\sim$0.03 photon at p = 1 torr. Consequently, at CF_4 pressure above 4 torr the rotational relaxation leads to absorption by all the gas molecules in the irradiated volume, and at p = 1 torr it operates only partially.

After reaching the maximum, the absorbed energy, starting with a certain pump-energy density (0.1 J/cm^2 and 2 J/cm^2 for p = 1 and 4.4 torr, respectively), decreases on the average and begins to undergo abrupt fluctuations of its absolute value. The relative scatter of the values of the absorbed energy in these cases reaches 200—400% within a measurement run at constant pumping, as compared with 10—20% at lower pump levels. This behavior agrees with the fluctuations observed in [37] of the lasing energy of a CF_4 laser, which were attributed to the nonreproducibility of the mode picture of the pump spectrum and to the degree of its agreement with the CF_4 absorption line spectrum. The decrease of the absorbed energy at a certain pump level was observed earlier for the OCS molecule and was attributed to participation of high vibrational levels in the absorption [41].

From our point of view, the absorption fluctuation shown in Fig. 22 can also be due to coherent interaction of the radiation with the absorbing medium (the self-transparency effect). A pulse of a CO_2 laser at atmospheric pressure, used to pump the gas, actually had a temporal fine structure, due to the self-locking of the modes that lie in the gain contour. The gain line width at p = 700 torr is $\sim$0.03 cm^{-1} and the duration of an individual pulse, assuming

full synchronization, is $\varepsilon_{pul} \sim 1$ nsec. A typical time of rotational relaxation is $p \cdot \varepsilon_{rot} \sim 30$ nsec·torr; therefore, at gas pressures of several torr the following coherence condition is satisfied:

$$\tau_{pul} \leqslant \varepsilon_{coh} = \tau_{rot} \tag{9}$$

The condition for observing coherent effects in absorption is

$$\frac{\mu}{\hbar} \int E(t)\, dt \geqslant 2\pi, \tag{10}$$

where μ is the dipole moment of the transition, $\hbar$ is Planck's constant, and E(t) is the electric field of the pulse.

Replacing the integral by the product $E_{max} \cdot \tau_{pul}$ and using the relation

$$I = \frac{c}{8\pi} E_{max}^2, \tag{11}$$

we obtain

$$I = \pi c \hbar^2 / 2\mu^2 \tau_{pul}^2, \tag{12}$$

where I is the pulse intensity and c is the speed of light. Substituting the values of the quantities at $\mu = 10^{-20}$ cgs esu and $\tau_{pul} = 10^{-9}$ sec, we find that

$$I \geqslant 5 \cdot 10^7 \ \text{w} \cdot \text{cm}^{-2}. \tag{13}$$

At a lasing line width 0.03 cm^{-1} and at a cavity length 3 m, the lasing pulse consists of $\sim$20 spikes of $\sim$0.6 J energy each. This yields an intensity in the spike 10^8 W/cm^2, i.e., coherent effects can take place. More accurate estimates call for a detailed knowledge of the temporal structure of the pulse and of the characteristics of the transition.

Thus, at high pump densities there can appear a self-transparency effect that decreases the absorption and, accordingly, the CF_4 laser energy. From this point of view, the scatter in the values of the absorbed energy is due to the nonreproducibility of the mode locking of the CO_2 laser. These effects can be avoided either by lowering the pump density at a given pressure, or by increasing the pressure at a constant pump. Consequently, at a given pressure there exists an optimal pump density and vice versa.

The maximum length of the CF_4 laser and the minimum pump energy density are determined, respectively, by the coefficient of the linear absorption and by the transition–saturation parameter. These quantities can be obtained from the dependence of the absorption on the input-energy density. As shown in [42], this dependence is determined by the formula

$$\ln\left(\frac{E_{in}^p}{E_{out}^p}\right) + \frac{1}{2E_s}\left(E_{in}^p - E_{out}^p\right) = \alpha_0 L, \tag{14}$$

where E_{in}^p and E_{out}^p are the pump energy densities at the input and output of the cell; E_s, saturation parameter; α_0, linear-absorption coefficient; and L, length of the gas layer.

As $E_{in}^p - E_{out}^p \to 0$ we have $\ln (E_{in}^p/E_{out}^p) \to \alpha_0 L$, and as $\ln (E_{in}^p/E_{out}^p) \to 0$ we have $(1/2)E_s \times (E_{in}^p - E_{out}^p) \to \alpha L$. Consequently, the dependence of $\ln (E_{in}^p/E_{out})$ on $E_{abs}^p = E_{in}^p - E_{out}^p$ makes it possible to determine both α_0 and E_s.

Such a dependence, at a pump frequency 1073.3 cm^{-1} and a CF_4 pressure 4.4 torr, is shown in Fig. 23. It yields the values $\alpha_0 = (2.0 \pm 0.5) \cdot 10^{-3}$ $cm^{-1} \cdot torr^{-1}$ and $E_s = (0.12 \pm 0.03)$ J/cm^2. The transition cross section, defined by the relation $\sigma N = \alpha_0$, is equal to $\sigma = (5.8 \pm 1.8) \cdot 10^{-20}$ cm^2. This value determines the saturation energy density $E_s^{(2)}$ under the condition that the rotational relaxation operates during the time of the pump pulse, $E_s^{(2)} = h\nu/2\sigma$. This relation gives $E_s^{(2)} = (0.18 \pm 0.05)$ J/cm^2. The proximity of the quantities $E_s^{(2)}$ to E_s

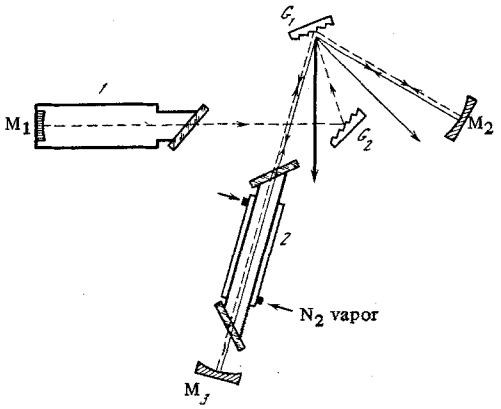

Fig. 24

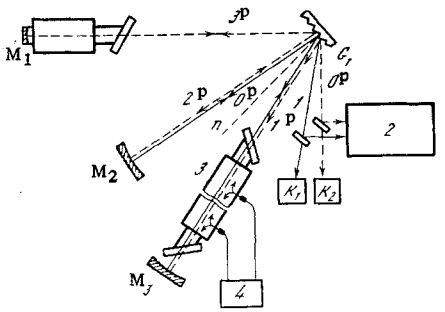

Fig. 25

Fig. 24. Optical system of CF_4 laser pumped by a CO_2 laser tunable in the lasing lines: 1) CO_2 laser; 2) NH_3 laser; solid lines — lasing; dashed — pump.

Fig. 25. Optical system of CF_4 laser pumped by CO_2 laser tunable within the 9R(30) line. Dashed arrows — pump; solid — lasing; 1) CO_2 lasers; 2) monochromator; 3) CF_4 laser; 4) cooling unit; n) normal to the surface of the diffraction grating; K_1, K_2) calorimeters.

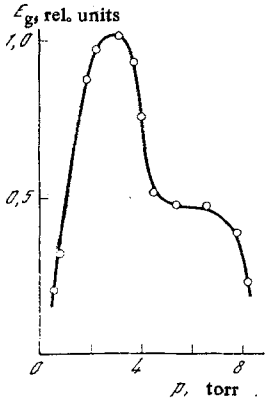

Fig. 26

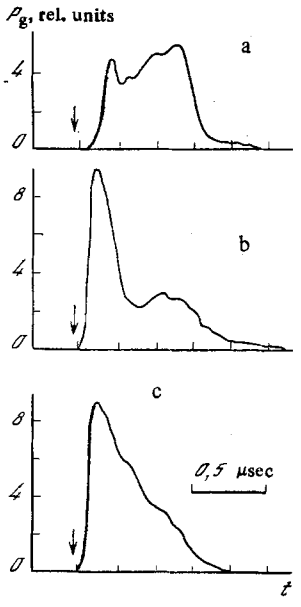

Fig. 27

Fig. 26. Dependence of the CF_4 laser emission energy on the gas pressure.

Fig. 27. Oscillograms of CF_4 laser pulses at various gas pressures: a) p = 2.4; b) 3.5; c) 4.5 torr. The arrow marks the maximum of the pump pulse.

indicates that at a pressure 4.4 torr the rotational relaxation is rapid enough to saturate the entire vibrational band. At lower values, E_s is contained in the range $E_s^{(1)} < E_s < E_s^{(2)}$, where $E_s^{(1)} = qE_s^{(2)}$, and q is the relative population of the given rotational level of the ground state. The dependence of the $\ln (E_{in}^p/E_{out}^p)$ on E_{abs}^p at a CF_4 pressure of 1 torr yields $E_s = 1.3$ mJ/cm^2. The upper limit of the factor q is given by the ratio E_s (1 torr)/$E_s^{(2)}$, i.e., q = 1/140.

The quantities α_0 and E_s obtained at a gas pressure 4.4 torr show that the optimal length of a CF_4 laser at this pressure is $\sim$10 m, and the threshold pump energy density is $\sim$0.1–0.2 J/cm^2.

3.2. Characteristics of the Emission of a CF_4 Laser. a. *Single-pulse regime.* The lasing was obtained by using the systems shown in Figs. 24, 25. The lasing was observed both visually and calorimetrically, using infrared filters that transmit either the pump radiation or the laser emission. In the system shown in Fig. 24, lasing was obtained in the pressure range 0.5–8 torr, and the maximum energy is observed at a CF_4 pressure of 3.5 torr (Fig. 26), in analogy with [37]. At low pressures, the lasing energy changes greatly from pulse to pulse, and when the pressure is increased these changes become smoothed out. Addition of helium or nitrogen to the cell decreased the pulse energy all the way to shutoff of the lasing at partial pressures of the buffer 5–6 torr. We note that covering the mirror M_2 did not stop the lasing, i.e., the energy is partially of superluminescence origin. The maximum registered lasing energy was 30 mJ.

The dynamics of the lasing is shown in Fig. 27. Just as for a laser, at low pressures the lasing pulse has two maxima. With increasing pressure the second maximum vanishes. This, as shown above, is due to the waveform of the pumping pulse from the CO_2 laser. The laser pumping pulse has an intense leading peak and a less-intense afterpulse. Therefore, at low CF_4 pressures the intensity reaches saturation both in the peak and in the afterpulse, while at higher pressures saturation is reached only in the peak.

Tuning of the CF_4-laser emission frequency in the range 612–650 cm^{-1} was achieved in [39] by varying the pump-radiation frequency with the aid of a germanium Fabry–Perot etalon. The low optical-breakdown strength and the problem of thermal stabilization of the etalon when working the described system in the periodic-pulse regime do not make its use possible at high pump powers.

In [28], systems were used in which there are no elements with low optical-breakdown strength. When using the system shown in Fig. 25, tuning was attained by pumping with different lines of the CO_2 laser. The results are given in Table 3.

It is known that in the CF_4 molecule the distance between the nearest absorption maxima at the composite mode $\nu_2 + \nu_4$ is 0.02–0.05 cm^{-1}, which is much less than the gain line width of an atmospheric-pressure CO_2 laser ($\sim$0.3 cm^{-1}). Thus, by tuning the CO_2 laser frequency within the gain line it is possible to excite the CF_4 to different rotational levels, and this makes it possible to tune the emission frequency of the CF_4 laser. To this end we used a compound CO_2 laser cavity, the diagram of which is shown in Fig. 25. The CO_2 laser was made up of mirror M_1, diffraction grating G_1 (50 lines/mm) operating in the autocollimation regime in the third order and tunable to a definite line of the CO_2 laser, and mirror M_2 perpendicular to the direction of the emission of the CO_2 laser in the second order of the grating G_1. The CO_2 laser frequency was tuned within the gain line by displacing the mirror M_2. The first-order radiation of the grating G_1 was directed into a cooled 3-m-long cell filled with CF_4. The radiation from the zeroth order was used to monitor the pump frequency. The pump energy was 8 J at a beam area 6 cm^2. The laser cavity was made up of mirrors M_3 and M_2, coupled through the zeroth order of the grating G_1. Radiation with $\lambda_g \approx 16$ μm emerged through the first order of the grating. The tuning results are given in Table 4.

b. *Periodic-pulse regime.* In [43] is described a CF_4 laser operating in the periodic-pulse regime with a pulse-repetition frequency up to 100 Hz.

Figure 28 shows the dependence of the lasing energy on the pulse-repetition frequency for three cases. The measurements were performed at pump-pulse energy $\sim$4 J. The absolute value of the pump energy decreased by approximately 12% upon addition of 0.5 torr of He, and decreased by 50% when 1 torr of He was added. It can be seen that a decrease of the lasing energy by one-half takes place at f = 17 Hz for pure CF_4 and at f = 75 Hz for a mixture with 1 torr of He. The lasing in the latter case was observed up to values f = 100 Hz. Figure 29 shows the obtained dependences of the average lasing power on the pulse repetition frequency. The maximum power amounted to 180 mW. It is possible to explain the behavior of the energy characteristics with increasing pulse-repetition frequency by considering the thermal regime of the lasing.

An estimate of the diffusion coefficient at the working temperatures and pressure gives a value D = 9 cm^2/sec, which makes it possible, without a noticeable decrease of the lasing energy, to change from the single-pulse regime to the periodic-pulse regime of the CF_4 laser

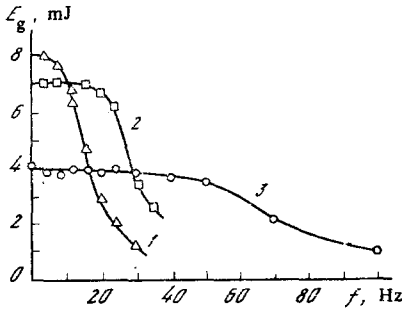

Fig. 28

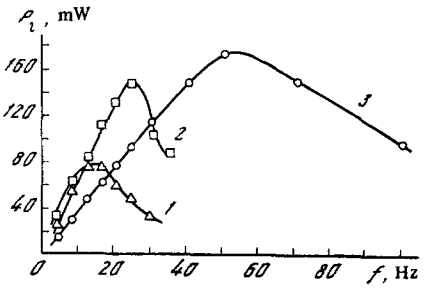

Fig. 29

Fig. 28. Dependence of the CF_4 laser pulse energy on the pulse repetition frequency at various pressures of the buffer gas (He): 1) pure CF_4 (2 torr); 2) with 0.5 torr of He added; 3) with 1 torr of He added.

Fig. 29. Dependence of the average CF_4 laser power on the pulse-repetition frequency at different pressures of the buffer gas (He): 1) pure CF_4 (2 torr); 2) with 0.5 torr of He added; 3) with addition of 1 torr of He.

TABLE 3

CO_2 laser line	ν_p, cm^{-1}	ν_g, cm^{-1}
9R (8)	1070,4	642,7 ±1
9R (10)	1071,9	638,4 ±1
9R (12)	1073,3	615,3 ±0,4
9R (14)	1073,6	615,3 ±1
9R (16)	1076,0	645,5 ±1
		632,3 ±1
9R (18)	1077,3	644,5 ±1

TABLE 4

CO_2 laser line	ν_p cm^{-1}	ν_g, cm^{-1}	E_g, mJ
9R (12)	1073,3	616 ±1	40
9R (10)	1071,9	624 ±1	25
9R (10)	1071,9	630 ±1	5

at a pulse repetition frequency up to 6 Hz. With further increase of the frequency, the diffusion time for the given parameters of the CO_2 laser beam becomes less than the time interval between two successive pump-radiation pulses, the gas begins to heat up, and for thermostatically controlled walls and at a certain specified pulse repetition frequency, a stationary temperature distribution is established in the cell. Solution of the stationary heat-conduction equation for a cylindrically symmetrical Gaussian beam leads to the following expression for the temperature increment on the beam axis:

$$\Delta T(0)=\frac{\alpha p_0 e^{-\alpha z}}{4\pi\varkappa}\left[\ln\left(2\gamma\frac{r_0^2}{a^2}\right)-E_i\left(-2\frac{r_0^2}{a^2}\right)\right], \tag{15}$$

where α is the absorption coefficient; p_0, power measured at the input to the cell; $\varkappa$, thermal-conductivity coefficient; r_0, cell radius, a, laser-pump beam radius; γ, Euler constant; and z, coordinate along the beam axis.

Estimates made for values $\alpha \sim 2\cdot10^{-4}$ $cm^{-1}\cdot torr^{-1}$ and $\varkappa \sim 2\cdot10^{-5}$ cal/cm·sec·deg with allowance for the dependence of the lasing energy on the CF_4 gas temperature, given in [37], yield the following. At a pump pulse energy ~4 J at the entry into the cell (z = 0), a decrease of the lasing energy to half the value should be observed at a pulse repetition frequency f ≈ 17 Hz. If, however, the thermal conductivity coefficient is artificially increased, then it is possible to also increase the pulse repetition frequency. Thus, e.g., the thermal-conductivity coefficient of a mixture of 2 torr of CF_4 and 1 torr of He will be approximately 4 times larger than $\varkappa_{CF_4}$, and consequently a decrease of the lasing energy of such a mixture to one-half the value should be observed at f ≈ 70 Hz, as was indeed observed in experiment (Fig. 28). Thus, the thermal model explains sufficiently well the energy characteristics of a CF_4 laser operating in the periodic-pulsed regime with a large pulse repetition frequency.

3.3. Discussion of Results. The generation of a CF_4 laser takes place on the transition $\nu_2 + \nu_4 \rightarrow \nu_2$ (see Fig. 21), i.e., against the background of absorption in the band ν_4. This is possible only because the line structures of the lasing and absorption spectra are different. The absorbing background can in the general case limit the range of frequencies accessible to lasing, and making tuning the lasing frequency difficult. Absorption causes the inversion of the population on the rotational sublevels of the upper laser level, which is reached on account of rotational relaxation, not to lead to emission of energy. Since the selection rules permit simultaneously the transition $\nu_2 + \nu_4 \rightarrow \nu_4$, which has no absorption background (the frequency ν_2 is not active in the IR spectrum), it is a strong competitor of the laser transition and decreases the efficiency of the CF_4 laser.

At a CF_4 pressure of 3.3 torr and at a pump of 12 J, the energy absorbed, according to our data, is 0.8 J. This yields an efficiency in terms of the absorbed energy of $\sim$4%. This low value is due mainly to the rotational relaxation of the upper laser level and to the action of the competing transition. The influence of the rotational relaxation can be decreased by shortening the pump pulse. The competing transition can be suppressed by introducing into the gas a substance that absorbs in the 22-μm region.

The overall pump efficiency in quite small, owing to ineffective use of the CO_2 laser energy. This effectiveness can be increased by several methods: matching the pump and absorption spectra using a single-frequency stable CO_2 laser, increasing the pump beam cross section, increasing the length of the CF_4 laser, and using an amplifier.

The specific energy of the laser in our case reached 0.03 J/liter. If it is assumed that the pump transfers 50% of all the molecules to the upper laser level and the population of the lower level is small, then at a pressure of 3.5 torr the stored specific energy is 1.3 J/liter. The rotational relaxation, the competing transitions, and other factors cause the specific energy of the lasing not to exceed 10—20% of the stored energy, i.e., $\sim$0.2 J/liter. Consequently, to obtain higher energy levels it is necessary to increase the volume of the active medium.

The repetition frequency of a CF_4 laser, and consequently also the average power, can be increased by having the CF_4 gas flow through at a rate at which the entire gas in the cell is replaced within the time between two successive pulses. In our case this rate amounts to $\sim$400 liter/sec at f = 100 Hz. However, as shown by the results above, no noticeable decrease of energy takes place up to f = 10 Hz, i.e., the required flow-through rate will be at least one order of magnitude lower.

One other method of increasing the average power is optimal utilization of the laser-cell volume. If we put in Eq. (15) $a = r_0$, then the lasing energy will decrease to half its value not at f = 17 Hz, but at f $\simeq$ 45 Hz.

Thus, it can be seen from the foregoing investigation that when a periodically pulsed CO_2 laser is used as the pump source, it is possible to obtain lasing in the 16- m band with an average power up to 200 mW and a pulse repetition frequency up to 100 Hz even without continuous flow of the CF_4 gas. Clearly, these parameters are not the limit. By continuous gas flow, by optimal utilization of the cell volume, by increasing the length of the cell (the length is limited by the absorption and by the divergence of the CO_2 laser), and by increasing the pump energy (no saturation was observed up to 5 J), it is possible to increase substantially the average lasing power of a CF_4 laser.

4. Use of NH_3 and CF_4 Lasers

4.1. Isotopically Selective Dissociation of the CCl_4 Molecule. Isotopically selective dissociation of the CCl_4 by radiation of an NH_3 laser with a frequency lower than that of the CO_2 customarily employed for this purpose was first realized in [44]. The optical system of the excitement is shown in Fig. 30.

A spherical mirror M_3 (F = 0.5 m, R = 98%) and a lens L_1 (F = 10 cm) focused the NH_3 laser radiation inside a cell with CCl_4. The effective focal length of the system of M_3 and L_1, measured from the plane of the lens L_1, was 6 cm. The energy density at the focus in this case reached 5 J/cm^2.

In an investigation of two-frequency dissociation of the CCl_4, part of the CO_2 laser radiation, reflected from a NaCl window, was focused with the aid of grating G and flat

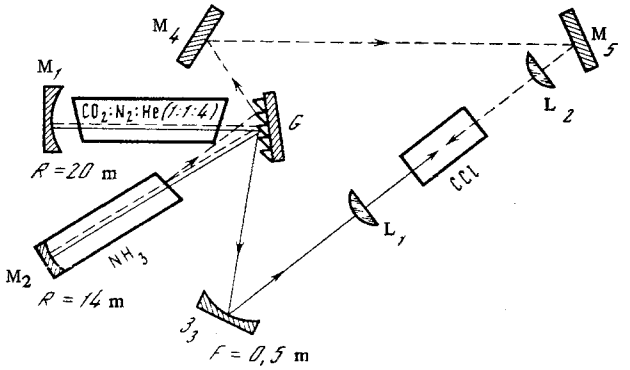

Fig. 30. Optical system of an experiment on the dissociation of a CCl_4 molecule by radiation of an NH_3 laser.

mirrors M_4, M_5 and lens L_2 (F = 20 cm) into the same region of the cell with CCl_4 as the radiation of the ammonia laser. The energy density at the focus reached 17 J/cm^2. In a number of experiments, the NH_3-laser radiation was focused only by the mirror M_3, and the energy density at the focus reached 1.6 J/cm^2.

The cell for the CCl_4 was made of stainless steel with KBr windows and had a length 12 cm and an inside diameter 1.2 cm. The evacuation and filling of the cell were with the aid of a vacuum system with residual pressure $p_{res} \sim 10^{-2}$ torr. The CCl_4 samples used were of natural isotopic composition as well as with enrichment (ratio $^{12}C:^{13}C$ = 38:62). Prior to the filling, additional cleaning was effected by vacuum distillation.

The rate of dissociation of the CCl_4 molecules was defined as

$$W = \frac{1}{n} \ln \frac{N_0}{N}, \tag{16}$$

where n is the number of irradiation pulses; N_0 and N are the initial and final concentrations of the molecules. The ratio of the concentrations N_0/N was determined from the IR absorption spectrum of the CCl_4. An isotopic analysis of the gas before and after the irradiation was carried out with a mass spectrometer.

Dissociation of the CCl_4 molecule under the action of a strong IR field of a CO_2 laser on the composite oscillation $\nu_1 + \nu_2 + \nu_4$ was investigated in [45]. The rate of the dissociation reached $2 \cdot 10^{-4}$ at a radiation energy density at the lens focus 120–150 J/cm^2. Enrichment of the dissociation products with the isotropes ^{13}C and ^{37}Cl was registered.

Our experiments have shown that the CCl_4 molecule dissociates under the influence of an ammonia laser radiation at the frequency ν = 780.5 cm^{-1}. The threshold energy density is in the range 1.6–2.0 J/cm^2. Above the threshold, the dissociation rate depends on the intensity I like $W \sim I^{4\pm1}$. At an energy density at the lens focus 4.0 J/cm^2, $\approx 2 \cdot 10^{-4}$ of the CCl_4 molecules located in the cell at the initial pressure 1.0 torr dissociate per pulse. This corresponds to a dissociation rate W = 0.04 for molecules located in a volume with energy density above the threshold. At higher intensities, W reaches 0.1. These figures show that the effectiveness of dissociation of CCl_4 upon excitation of the fundamental oscillation ν_3 is 2–3 orders higher than upon excitation of the compound oscillation $\nu_1 + \nu_2 + \nu_4$, despite the considerable detuning of the NH_3 laser (780.5 cm^{-1}) from the ν_3 oscillation frequency (796 cm^{-1}).

So high an effectiveness can be explained by the fact that the NH_3-laser frequency lands in the quasicontinuum produced by the absorption of vibrationally excited molecules [46]. It is known from experiment that this region spans a wide range of the spectrum, shifted into the low-frequency side relative to the spectrum of the linear absorption of the molecules [47].

Figure 31 shows the dependence of the dissociation rate on the initial CCl_4 pressure. Unlike all other known cases [46], this curve shows a minimum at a pressure $\sim$0.25 torr. The course of the curve in the low-pressure region agrees qualitatively with the analogous

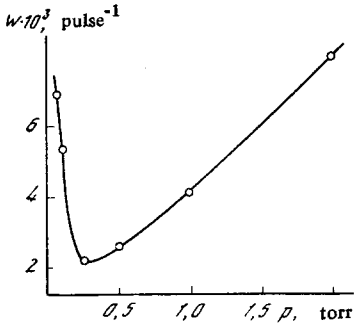

Fig. 31

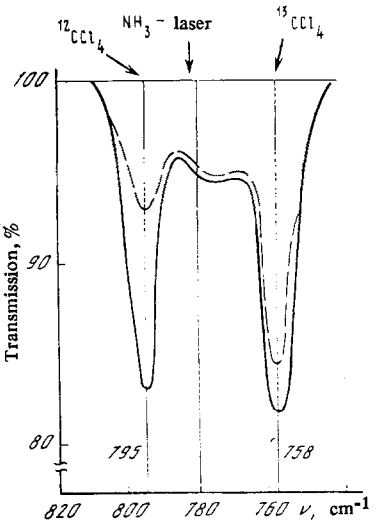

Fig. 32

Fig. 31. Dependence of the dissociation rate per pulse on the CCl_4 pressure. The energy density at the focus is 4.5 J/cm^2.

Fig. 32. Selective dissociation of CCl_4 enriched with the isotope ^{13}C ($^{12}CCl_4$:$^{13}CCl_4$ = 38:62). Solid curve — IR absorption spectrum of CCl_4 prior to irradiation. Dashed line — IR spectrum after irradiation (CCl_4 pressure 0.25 torr, energy density at the focus 5 J/cm^2).

dependence for SF_6 [48] and is due to the quenching action of the collisions on the acquisition of energy by the molecules. At a pressure higher than 0.25 torr the dissociation rate of the CCl_4 increases with increasing pressure. The plot of W(p) in the section 0.25–2.0 torr is practically linear. It appears that the principal role is played here by the increase of the number of molecules that absorb energy, possibly on account of thermal heating during the time of the pulse.

Besides the dissociation rate, an important feature is isotopic selectivity. In our measurements we used a CCl_4 sample enriched with ^{13}C. This lowered the influence of the parasitic peaks and made it possible to measure the selectivity by two independent methods: by determining the mass spectrum of the dissociation products, and by using the IR spectrum of the residual gas. In the first method the selectivity S was determined by the ratio of the peaks of $^{12}C^{13}CCl_3^+$, $^{13}C_2Cl_3^+$ and $^{12}C^{13}CCl_4^+$, $^{13}C_2Cl_4^+$, while in the second it was determined by the ratio of the dissociation rates of the two isotopic modifications, $S = W(^{12}C)/W(^{13}C)$.

Figure 32 shows an example of isotopically selective dissociation of CCl_4. When enriched CCl_4 (p = 0.25 torr) was irradiated by 1300 pulses of an NH_3 laser with energy density at the focus 5 J/cm^2, the selectivity obtained was $S = 4.4 \pm 0.3$. The enrichment coefficient in the residual gas was 2.0 ± 0.1 at a total gas consumption ∿40%. A certain correlation was observed between the selectivity and the radiation energy density. Thus, the selectivity decreased to ∿2.8 at an energy density ∿4 J/cm^2. The selectivities with respect to the IR and mass spectra were recorded simultaneously. The initial gas pressure was 0.3 torr, and the total consumption 8%. The ratio of the dissociation rates was $S = 3.5 \pm 0.6$. The coefficient of enrichment of the products with the isotope ^{12}C was 4.5 ± 0.1 in accordance with the $C_2Cl_3^+$ peaks and 6.2 ± 0.2 in accordance with the $C_2Cl_4^+$ peaks. The respective coefficients of enrichments with the isotope ^{37}Cl were 1.12 ± 0.02 and 1.15 ± 0.02. The higher rate of dissociation of $^{12}CCl_4$ corresponds to enrichment of the products with the isotope ^{12}C. The difference between the values of the selectivity and the low absolute value point to a strong influence of secondary chemical reactions.

TABLE 5

ν, cm^{-1}	E^n, J/cm^2	W ($^{12}CCl_4$)·10^2	W ($^{13}CCl_4$)·10^2	ν, cm^{-1}	E^n, J/cm^2	W ($^{12}CCl_4$)·10^2	W ($^{13}CCl_4$)·10^2
Single-frequency regime				Two-frequency regime			
1075,9	17	0,1	0,1	780,5	4	13,4	—
	4	4,4	—	1075,9	17		
780,5	1,6	0,1	0,1	780,5	1,6	3,7	2,0
				1075,9	17		

We have also investigated a two-frequency dissociation regime. In this regime the entire process is divided into two stages: excitation and dissociation of the excited molecules. The first stage is effected by a relatively weak resonant radiation, and the second by a powerful nonresonant field. In the case of the NH_3 laser, it is convenient to use as the second field the radiation of the pumping CO_2 laser. Results of experiments at $p_{CCl_4} = 1$ torr are given in Table 5. At an NH_3 laser energy 1.6 J/cm^2 and at a CO_2 laser energy 17 J/cm^2 the dissociation rate of $^{12}CCl_4$ is $3.7 \cdot 10^{-2}$, and the selectivity in this case is 1.85. Control experiments have shown that each field by itself does not cause dissociation, to within the measurement error (10^{-3}). In experiments with sharp focusing of the NH_3 laser radiation, addition of the nonresonant field of the CO_2 laser increased the rate of dissociation by 3.1 times.

Consequently, the two-frequency regime makes it possible to obtain a dissociation efficiency comparable with the single-frequency variant, with less stringent requirements on the energy density of the ammonia laser. These results were obtained at a nonresonant radiation-frequency detuning by ∿300 cm^{-1} toward the high-frequency side (∿40% of the NH_3 laser frequency). The decrease in the selectivity is apparently due to its noted dependence on the energy density of the NH_3 laser at a given pulse duration.

Our experiments represent the first case when radiation with a wavelength longer than that of the CO_2 laser was used for dissociation. The efficiency of the process is very high: up to 10% of the molecules located in the volume, with energy density above threshold, dissociate in one pulse. Such a yield was reached at a large detuning of the NH_3 laser frequency and one of the ν_3 oscillation of the $^{12}CCl_4$ molecule (∿15 cm^{-1}). The explanation of this fact is the following: the spectra of the transitions between the excited levels has shifted from the oscillation frequency of the molecule by 10–20 cm^{-1} to the "red" side because of the anharmonicity, but the detuning should be directed toward the lower frequency.

To increase the selectivity it is necessary to establish both transfer of the vibrational excitation during the time of the pulse and an influence of secondary chemical reactions. To this end it is necessary to operate at low pressures of the CCl_4 (≤0.1 torr) in the presence of an optimal acceptor for the radicals.

4.2. Comparison of the Efficiency of the Excitation of Various Types of Molecule Vibrations. The possibility of exciting with the aid of an NH_3 laser the fundamental vibration ν_3 of the CCl_4 molecule, and with the aid of a CO_2 laser the composite vibration $\nu_1 + \nu_2 + \nu_4$, has made it possible to compare the effectiveness of the activation of the molecule when a high-power field acts on these vibrational modes. In [49] is contained an experimental comparison of the mean values of the energy absorbed by the CCl_4 molecule upon excitation of the modes ν_3 and $\nu_1 + \nu_2 + \nu_4$ to the dissociation level. The action on the composite vibration $\nu_1 + \nu_2 + \nu_4 = 980$ cm^{-1} was produced by radiation of a CO_2 laser (line 10P(26)). The fundamental vibration $\nu_3 = 794$ cm^{-1} was excited by an NH_3 laser pulse at a frequency $\nu = 771$ cm^{-1}. The temporal shapes of the pulses were in qualitative agreement. The CCl_4 pressure was 0.5 torr. The radiation was focused into the interior of a cell by a KBr lens with focal length 10 cm. The absorbed energy was determined by an optoacoustic receiver. The construction of the receiver made it possible to carry out the measurements directly in the focal plane of the lens.

To compare the absorbed energy upon excitation of different modes of the CCl_4 molecule it is necessary to ensure an equal excitation level; this was done at a field excitation intensity equal to the dissociation-rate threshold. Figure 33 shows the dependence of the dissociation rate of the CCl_4 molecule on the incident energy. The values of the threshold

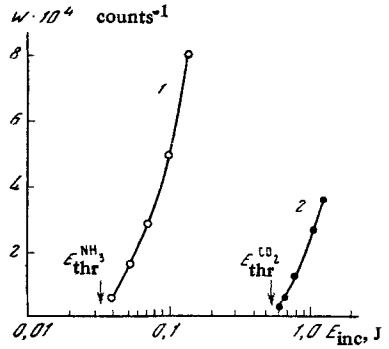

Fig. 33

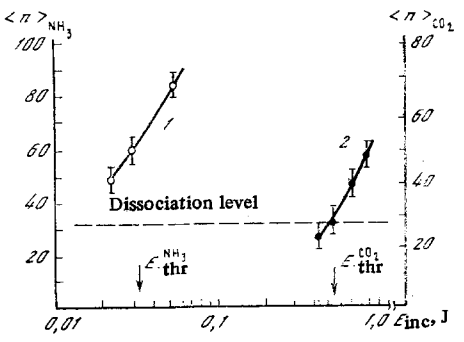

Fig. 34

Fig. 33. Dependence of the degree of dissociation of the CCl_4 molecule on the laser energy incident on the cell: 1) NH_3 laser; 2) CO_2 laser.

Fig. 34. Dependence of the average number of IR-emission photons absorbed by the CCl_4 molecule on the energy incident on the cell: 1) for NH_3 laser; 2) for CO_2 laser.

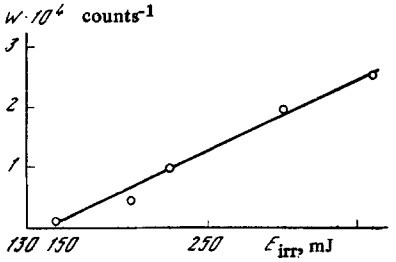

Fig. 35

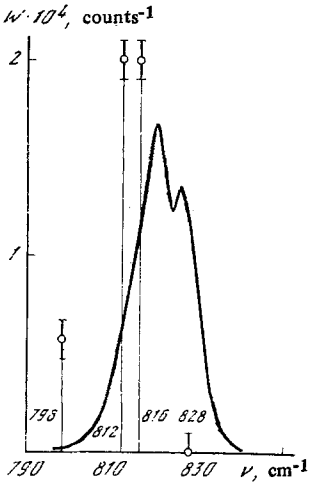

Fig. 36

Fig. 35. Dependence of the UF_6 dissociation yield on the energy in the pulse at a frequency 816 cm^{-1}.

Fig. 36. Spectral dependence of the dissociation yield in the linear absorption spectrum of the UF_6 molecule. The irradiation energy is 300 mJ.

energies were 1.2 J/cm^2 and 120 J/cm^2 when the ν_3 and $\nu_1 + \nu_2 + \nu_4$ modes were excited, respectively.

The fraction q of the captured particles was determined by the method of two-frequency saturation of the dissociation yield [50]. The nonresonant laser was an ultraviolet XeCl excimer laser. It turned out that the value of q is close to unity for both the CO_2 and the NH_3 laser.

Figure 34 shows the dependence of the average number of photons absorbed by a CCl_4 molecule on the irradiation energy. It can be seen that when the mode ν_3 is excited to the dissociation level, the molecule absorbs twice as many IR photons as when the composite vibration is excited.

It has thus been shown experimentally that the energy needed to excite a molecule to the dissociation limit depends substantially on the type of excited oscillation. This fact, together with the need for shifting the laser-radiation wavelength into the "red side" relative to the linear-absorption band, is a condition of fundamental importance for the increase of the quantum yield of the products in multiphoton dissociation in a high-power IR field.

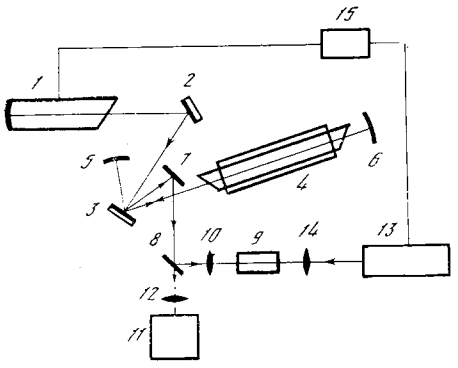

Fig. 37

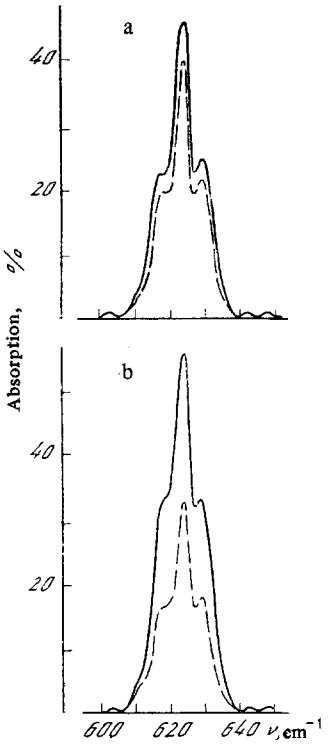

Fig. 38

Fig. 37. Optical diagram of experiment on dissociation of a UF_6 molecule by emission from CF_4 and N_2 lasers: 1) CO_2 laser; 2, 3) diffraction gratings; 4) CF_4 laser; 5-8) mirrors; 9) cell with UF_6; 10, 12, 14) lenses; 11) calorimeter; 13) N_2 laser; 15) block for synchronization of the CO_2 and N_2 lasers.

Fig. 38. IR absorption spectrum of UF_6 prior to irradiation (solid curve) and after irradiation (dashed curve); a) irradiation by CF_4 laser; b) combined irradiation by CF_4 and N_2 lasers.

4.3. Dissociation of Uranium Hexafluoride by NH_3-Laser Radiation. For further investigation and comparison with the efficiency of excitation of different types of vibrations, experiments were performed in [51] on the dissociation of UF_6 molecules irradiated by an NH_3 laser. The dissociation upon excitation of the fundamental vibration ν_3 at the frequency 615 cm^{-1} was investigated in [52]. In our experiments, the NH_3 laser radiation excited the composite vibration $\nu_3 + \nu_5$ (824 cm^{-1}). We used lines with frequencies 828, 816, 812, 798 cm^{-1}. The experiments were performed at a pressure 0.5 torr. The radiation of the NH_3 laser was focused by a KBr lens of focal length 20 cm into a spot of area 1.5 mm^2.

The dissociation yield W was defined as $W = \frac{T}{n}\left(\frac{1}{T}\frac{N_0}{N_1} - \frac{1}{\tau}\right)$, where N_0 and N_1 are the initial and final molecule densities, determined from the IR absorption spectra at a frequency 625 cm^{-1}, n is the number of irradiation pulses, T is the irradiation time ($\approx$1 h in the experiment), and $1/\tau$ is the "natural" decrease of the matter ($1/\tau \leqslant 0.04$ h^{-1}) due to passivation of the cell and window material.

Figure 35 shows the dependence of the dissociation yield on the incident radiation energy of frequency 816 cm^{-1}; it is seen to be practically linear. The dissociation threshold was 150 mJ or 10 J/cm^2, i.e., only several times larger than for the excitation of the ν_3 mode [52]. At an irradiation energy E_{irr} = 500 mJ (33 J/cm^2) the dissociation yield is $4 \cdot 10^{-4}$ per count, and in this case $\sim$0.01 of all the molecules contained in the volume where the energy density exceeds the threshold are dissociated, i.e., the efficiency is 1%. At an energy 300 mJ (20 J/cm^2) the dissociation yield is $2 \cdot 10^{-4}$ per count at an efficiency $\sim$8%. The increase of the dissociation efficiency with decrease of the energy density is due to the decrease of the fraction of the volume with low radiation density.

To determine the spectral characteristics of the efficiency of multiphoton excitation of UF_6 molecules, investigations were made of the dependence of the dissociation yield on the NH_3-laser radiation frequency. In these experiments the radiation energy was 300 mJ. The results are shown in Fig. 36. As usual, upon excitation of the composite vibration $\nu_3 + \nu_5$ the maximum of the dissociation of UF_6 is shifted, relative to the spectrum of the linear absorption, into the "red" direction by 7.5 cm^{-1}.

The addition of hydrogen as an acceptor to the UF_6 did not significantly increase the dissociation yield. This can be attributed either to the fact that in the absence of hydrogen the dissociation products are completely bound by the residual-gas molecules (the residual gas pressure is $\sim 2 \cdot 10^{-2}$ torr), or to detachment of the F_2 molecule, which does not react with the H_2, from the UF_6 molecule.

The investigations have shown that UF_6 molecules can be effectively dissociated by laser radiation, by exciting the composite modes.

4.4. Dissociation of Uranium Hexafluoride by Radiation of a CF_4 Laser. The availability of a CF_4 laser generating at 616 cm^{-1} has made it possible to perform an experiment on the dissociation of UF_6 in accordance with the one- and two-step systems [53]. The experimental setup (Fig. 37) consisted of a CF_4 laser optically pumped by a CO_2 laser, an N_2 laser, and a vacuum system with working cells and auxiliary equipment. The CF_4 laser was pumped by radiation at the frequency of the 9R(12) line of the CO_2 laser (frequency 1073.38 cm^{-1}). The CF_4 laser frequency was 615.3 ± 0.6 cm^{-1}. The average radiation energy was 10–12 mJ. The source of the UV radiation was a nitrogen laser with transverse discharge and emission energy ~ 2 mJ. The UV radiation pulse was delayed ≈ 700 nsec relative to the IR pulse.

The emission of the CF_4 laser was guided by mirrors into the working cell and was focused with a KBr lens. The focal length of the lens was 5 cm in the single-frequency experiments and 20 cm in the two-frequency experiments. From the opposite side of the quartz lens with F = 20 cm, radiation of the CF_4 laser was focused into the cell. The foci of the lenses were superimposed in such a way that the UV radiation covered in all cases the region of the caustic of the IR radiation.

The change in the UF_6 content in the cell was determined from the IR absorption spectra.

In the experiment the photodissociation yield W was measured when the gas was irradiated by each laser separately, and also in the two-step scheme "IR excitation + UV dissociation." The value in the case of the action of the UV radiation did not exceed 10^{-6}. On the contrary, the IR dissociation is quite noticeable: the yield per pulse is $(5...7) \cdot 10^{-5}$ at a pulse energy 8–10 mJ at the entry to the cell and at a focal length of the lens 5 cm (Fig. 38a). When the radiation energy was decreased or the focal length increased, the yield decreased rapidly. The estimate obtained in this manner for the threshold energy density yielded a value 1–2 J/cm^2. Despite the small values of W, the dissociation yield in the region with energy density above the threshold is quite high: it reaches $\approx 20\%$ at a focal density ≈ 5 J/cm^2.

The degree of utilization of the CF_4 laser and the dissociation yield increase substantially when the two-step scheme is used. In this experiment the lens with F = 5 cm was replaced by a lens with F = 20 cm. Under these conditions there was no photodissociation, accurate to the measurement error. At the same time, addition of UV radiation caused a substantial increase in the gas flow (Fig. 38b). The value of W in these experiments reached $(3... 3.5) \cdot 10^{-4}$.

The results uncover a possibility of studying the dissociation of uranium hexafluoride by IR-laser radiation, and also of continuing the research into the effectiveness of excitation of various types of vibrations in molecules.

APPENDIX

1. The operation of an optically pumped laser can be analyzed with the aid of the rate equations. For the optical pumping scheme in which the radiation of the CO_2 laser is converted in NH_3 molecules (see Fig. 1a), the system of rate equations for the level populations and for the pump and lasing fields can be written in the form

$$\frac{\partial n_1}{\partial t}=(n_2-n_1)W_p+(q_1N_0-n_1)\frac{1}{\tau_{rot}^0},$$

$$\frac{\partial n_2}{\partial t}=(n_2-n_1)W_p-(n_2-n_3)W_g+\frac{q_2N_1-n_2}{\tau_{rot}^1},$$

$$\frac{\partial n_3}{\partial t}=(n_2-n_1)W_g+\frac{q_3N_0-n_3}{\tau_{rot}^0},\qquad \frac{\partial N_0}{\partial t}=(n_2-n_1)W_p+(n_2-n_3)W_g+\frac{N_1}{\tau_{V-T}},$$

$$\frac{\partial N_1}{\partial t}=-(n_2-n_1)W_n+(n_2-n_3)W_g-\frac{N_1}{\tau_{V-T}}-N_1W_V,$$

$$\frac{\partial W_g^+}{\partial t}=-\frac{W_g^+}{\tau_{res}}+(n_2-n_3)h\nu_pB_{23}g(\nu)W_g^+-c\frac{\partial W_g^+}{\partial z}, \tag{17}$$

$$\frac{\partial W_g^-}{\partial t}=-\frac{W_g^-}{\tau_{res}}+(n_2-n_3)h\nu_gB_{23}g(\nu)W_g^-+c\frac{\partial W_g^-}{\partial z},$$

$$\frac{\partial W_p}{\partial t}=-(n_1-n_2)h\nu_pB_{12}g(\nu)W_p-c\frac{\partial W_p}{\partial z},$$

where n_1, n_2, and n_3 are the populations of the rotational sublevels, the transitions between which cause the absorption of the pump radiation (transition $1 \to 2$) and lasing (transition $2 \to 3$); N_0, number of particles in the ground state, equal to the sum of particles in all the rotational sublevels of the ground state of the given mode; N_1, sum over all the rotation sublevels of the excited state of the same mode; W_p, W_g, rates of stimulated transitions between the sublevels in the pump and generation fields, respectively; τ_{rot}^0, τ_{rot}^1, times of rotational relaxation to the equilibrium distribution over the sublevels of the ground and excited states.

The equations for N_0 and N_1 take into account terms that describe the vibrational–translational relaxation with a time τ_{V-T} and the intermode exchange with a time W_{V-T}, which leads to a change in the number of particles in the given mode. The geometry of the optical pumping is shown in Fig. 39. At the origin is located a selective mirror transparent to the pump radiation and having a reflection coefficient R for the lasing radiation. At the point z = L the mirror is transparent to the pump radiation and is opaque to the stimulated emission of the NH_3 laser. The lasing field is regarded as the sum of two waves. W_g^+ is the rate of stimulated transitions in the field of the wave propagating in the direction of the z axis, and W_g^- is the rate of the stimulated transitions in the field of the wave propagating in the direction of the negative z axis, with $W_g = W_g^+ + W_g^-$. The pump wave in such a geometry propagates only in the direction of the z axis. The rate of the stimulated transitions between the levels i and j in a radiation field with intensity I is

$$W_{ij}=\sigma_{ij}\frac{I}{h\nu_{ij}}, \tag{18}$$

where ν_{ij} is the transition frequency; $\sigma_{ij} = g(\nu)B_{ij}(h\nu_{ij}/c)$, transition cross section; $g(\nu)$, line shape, which can be determined by the Doppler broadening at low pressures, or by the collision broadening at high pressures; and B_{ij}, Einstein coefficient for the stimulated transitions.

We consider in this paper the stationary case $\partial/\partial t = 0$ under the assumptions $\tau_{rot}^0 \sim \tau_{rot}^1$ and $\tau_{V-V'} >> \tau_{V-T}$. The last assumption makes it possible to neglect the $V–V_1$ exchange, and in this case it follows from the equations for N_0 and N_1 that $N_0 + N_1 = \text{const} = N$ is the total number of particles per unit volume. From the equations for W_g^+ and W_g^- follows one more integral of the system: $W_g^+W_g^-$ = const, i.e., it is independent of z. The constant is obtained from the boundary conditions on the mirrors, which take the form $W^+(L) = W^+(L) = W^-(L)$, $RW^-(0)$. The system (17) for the stationary case and for the indicated relations between the relaxation times can be written in the form

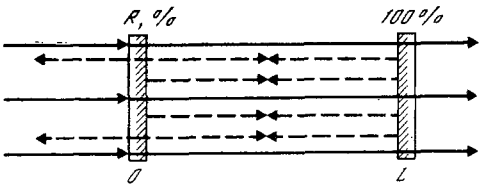

Fig. 39

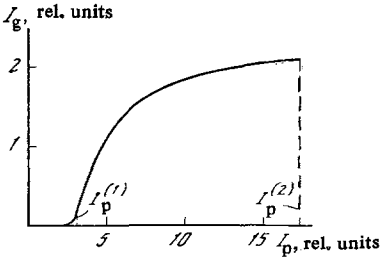

Fig. 40

Fig. 39. Geometrical scheme of optical pumping used to calculate the characteristics of the NH_3 laser. Solid lines – pump; dashed – lasing.

Fig. 40. Calculated dependence of the lasing intensity of an NH_3 laser on the pump-pulse intensity.

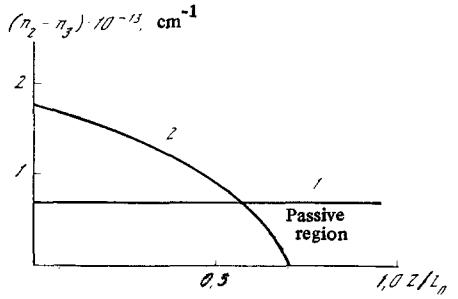

Fig. 41

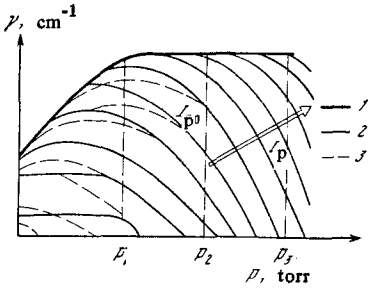

Fig. 42

Fig. 41. Calculated dependence of the distribution of the population inversion over the length of the cell of the NH_3 laser for the peak intensity (1) and for the maximum intensity on the "tail" of the pump pulse (2).

Fig. 42. Dependence of the gain on the pressure of the active medium and on the pump intensity [13] (logarithmic scale): 1) maximum gain; 2) gain for broadband pumping; 3) gain for monochromatic pumping. The arrow shows the increase of the pump intensity.

$$
\begin{aligned}
&(n_2 - n_1) W_p + (q_1 N_0 - n_1) \frac{1}{\tau_{rot}} = 0, \quad -(n_2 - n_1) W_p - (n_2 - n_3) W_g + q^2 \frac{N_1 - n_2}{\tau_{rot}} = 0, \quad (n_2 - n_3) W_g + \frac{q_3 N_0 - n_3}{\tau_{rot}} = 0,\\
&(n_2 - n_1) W_1 + (n_2 - n_3) W_g + \frac{N_1}{\tau_{V-T}} = 0, \quad N_0 + N_1 = N,\\
&-\frac{W_g^+}{\tau_{res}} + (n_2 - n_3) h\nu_g B_{23} g(\nu) W_g^+ - c \frac{\partial W_g^+}{\partial z} = 0, \quad W_g^+ W_g^- = W_g^2 + (0),\\
&-(n_1 - n_2) n\nu_p B_{12} g(\nu) W_p - c \frac{\partial W_p}{\partial z} = 0,
\end{aligned}
\tag{19}
$$

The system of equations (19) was solved by numerical methods. In the calculation we used the following values of the parameters: τ_{rot} = 1 nsec, τ_{V-T} = 40 nsec, mixture NH_3:N_2 = 1:75 at a total pressure p_Σ = 60 torr. The results of the calculation are shown in Fig. 40. The maximum intensity of the pump corresponds to the intensity at the peak of the pump pulse. It can be seen that at this intensity the lasing intensity saturates, i.e., the intensity of the lasing pulse does not increase with increasing intensity at the peak of the pump pulse, i.e., part of the pulse with intensity higher than the saturation intensity is not used, as was indeed observed experimentally in the present study. The dependence of I_q on I_p has a clearly pronounced threshold character; when the intensity in the pump pulse is less than I_{thr} the NH_3 laser shuts off, and it is this which explains why the lasing pulse is shorter than the pump pulse.

Figure 41 shows the calculated dependences of the distribution of the population inversion (n_2-n_3) over the length of the NH_3-laser cell for a peak intensity I_{peak} and for the maximum intensity on the tail of the pump pulse. It can be seen that at an intensity $I_p = I_{peak}$ the inversion does not depend on z. The saturation of the absorption is observed along the entire cell. At a lower intensity, a region is produced where $n_2-n_3 < 0$, the so-called passive region, which causes active losses in the NH_3-laser cavity. With decreasing intensity, the passive region increases, and in this case the lasing energy decreases and eventually the laser shuts off. Thus, the obtained experimental characteristics of the NH_3 laser are fully explained on the basis of the solution of the system of rate equations.

Solution of the nonstationary system of equations (17) will make it possible to explain in the future the temporal characteristics of the lasing pulse and to draw conclusions concerning the limiting parameters of the NH_3 laser.

The gain of the active medium in the case of optical pumping is determined by three basic independent parameters: 1) the density N of the molecules (cm^{-3}), i.e., the gas pressure $p \sim N$; 2) the pump intensity I_p; 3) the detuning $\delta\nu_p^d$ of its frequency ν_p relative to the center of the pump absorption line ν_{13}

$$\delta\nu_p^d = \nu_p - \nu_{13}. \tag{20}$$

This dependence is shown in general form in Fig. 42. It also implicitly contains a number of other parameters which are themselves functions of p and I_p. These are primarily the widths of the two spectral lines, $\Delta\nu_p \equiv \Delta\nu_{13}$ and $\nu_l \equiv \Delta\nu_{32}$. The line with $\Delta\nu_p = \Delta\nu_{13}$ corresponds to the transition $1 \to 3$ excited by the pump, and the line with $\Delta\nu_p = \Delta\nu_{32}$ corresponds to the laser (working) transition $3 \to 2$ (see Fig. 18). The quantities $\Delta\nu_p$ and $\Delta\nu_l$ are determined by the relation between the two broadening factors. These are the Doppler broadening

$$\Delta\nu_{p,l}^D = 3 \cdot 18 \cdot 10^{-7} \sqrt{T/M} \cdot \nu_{p,l}, \tag{21}$$

where T is the temperature, °K, and M is the molecular weight, and the collisional broadening

$$\Delta\nu_{p,l}^{imp} \approx N \langle \sigma v \rangle, \tag{22}$$

where σ is the collision cross section, v is the molecule velocity, and $\langle\sigma v\rangle$ denotes averaging over the Maxwellian distribution.

In Fig. 42, p_1 denotes the pressure at which the collisional broadening $\Delta\nu_l^{imp}$ of the laser transition becomes equal to the Doppler width $\Delta\nu_l^D$ of the laser transition:

$$\Delta\nu_l^{imp} = \Delta\nu_l^D. \tag{23}$$

The pressure p_2 corresponds to the analogous situation with respect to a transition excited by the pump radiation

$$\Delta\nu_p^{imp} = \Delta\nu_p^D. \tag{24}$$

The pressure p_3 corresponds to the equality

$$\Delta\nu_p^{imp} = \delta\nu_p^d, \tag{25}$$

where $\delta\nu_p^d$ is the detuning of the pump from resonance.

From (21)-(24) we obtain

$$N_{p_1,p_2} = \frac{3.58 \cdot 10^{-7} (T/M)^{1/2} \nu_{l,p}}{\sigma v}. \tag{26}$$

Since $\nu_p > \nu_l$ and $\delta\nu_p^d > \Delta\nu_p$, $\Delta\nu_l$, it is obvious from (25) and (26) that $p_1 < p_2 < p_3$ with $p_1/p_2 = \nu_l/\nu_p$. The interval $p_1 < p_2$ is the low-pressure region, $p_1 < p < p_2$ is the medium-pressure region, and $p_1 > p_2$ is the high-pressure region.

In the low-pressure region ($p < p_1$) the gain $\gamma = \sigma_l N$ at any pump, even the most intense, is proportional to the pressure $p \sim N$ and corresponds to the envelope of the curves of Fig. 42. In fact, the gain $\gamma \sim N/\Delta\nu_l$, so that γ increases with increasing $p \sim N$, since the growth of N is not offset by the broadening $\Delta\nu_l$: in the region $p < p_1$ the width of the laser transition is $\Delta\nu_l \simeq \Delta\nu_l^D = \text{const}$. In the region of medium and high pressures, the maximum gain is independent of pressure. Indeed, e.g., at $p_1 < p < p_2$, when the pressure is increased the increase of the density of the active particles is offset by the collisional broadening of the line of the laser working transition, since $\Delta\nu_l \simeq \Delta\nu_l^{imp} \sim N$.

If the pump intensity is fixed, the pressure dependence has a characteristic maximum: the gain first increases, and then begins to decrease. The reason for this is the following. With increasing pressure (at a fixed pump intensity) this intensity becomes insufficient to ensure saturation over the entire length. In fact, at $p_1 < p < p_2$ the absorption coefficient increases with pressure: the increase of the molecule density N is not offset by the collisional broadening of the absorption line, since we still have $\Delta\nu_p^{imp} < \Delta\nu_p^D$. Consequently, the pump absorption coefficient $\alpha = \sigma_p N$ increases. The length of the excited part of the active region, L_{exc}, decreases in this case, since $L_{exc} \sim \alpha^{-1}$. On the other hand, the unexcited part of the active medium introduces losses into the generating-laser radiation because of the thermal population of the final laser level 2. (Each unexcited molecule of the active medium has an absorption cross section σ equal to the gain cross section $\sigma_{32} = \sigma_l$ of the excited molecule.) In other words, if the pulsed* pump is incapable of pumping the entire length of the active medium, its unexcited part will play the role of the active losses.

If the pump does not ensure a saturation regime, the volume excitation velocity w_p $(\text{cm}^{-3}\cdot\text{sec}^{-1}) = I_p\alpha \sim I_p N\Delta\nu_{12}^{-1}$, since $\alpha \sim N\Delta\nu_{13}^{-1}$, where $N \simeq N_1$. On the other hand, the gain of the laser working transition is

$$\gamma \sim w_p\tau_3\Delta\nu_{32}^{-1} = I_p\tau_3 N\Delta\nu_p^{-1}\Delta\nu_l^{-1}, \tag{27}$$

where $\tau_3 \sim N^{-1}$ is the lifetime on the upper level and $\Delta\nu_{32} = \Delta\nu_l$ is the width of the laser-transition line. In the high-pressure region ($p > p_3$), obviously, $\Delta\nu_p\Delta\nu_l \sim N^2$ and (at unsaturated pumping, as seen from (27)) the gain is $\gamma \sim I_p N^{-2}$. A different picture is observed at unsaturated pumping in the region of low ($p < p_1$) and medium ($p_1 < p < p_2$) pressures. In these pressure regions the gain depends on the line width $\delta\nu_p$ of the pump source. If the resonant pumping is broadband ($\delta\nu_p > \Delta\nu_{p_1}\Delta\nu_l$), the collisional broadening can be neglected in the low-pressure region $p < p_1$, and then $\Delta\nu_p\Delta\nu_l = \text{const}$. From this we obtain for the gain $\gamma \sim I_p$, i.e., the gain depends only on the intensity. At medium pressures ($p_1 < p < p_2$) we have $\Delta\nu_p\Delta\nu_l \sim N$ and $\gamma \sim I_p N^{-1}$.

The maximum gain that can be obtained at minimum pump corresponds to the pump intensity $I_p = I_{p0}$ and pressure $p = p_1$. This corresponds to the case when the pressure is still not

---

*In this case the energy density in the pump pulse E_p^{den} in insufficient to excite the active medium: $E_p^{den} < E_s$; indeed, $E_s \simeq 1/2\ LNh\nu_p$. For $p = 10$ torr, $N = 3.5\cdot10^{17}$ cm^{-3}, $h\nu = 2.5\cdot10^{-20}$ J, $L = 10^2$ cm, $E_s = 1/2\ 10^2\cdot3.5\cdot10^{17}\cdot2.5\cdot10^{-20} = 0.5$ J/cm^2.

high enough for the collisional broadening of the laser line to compensate for the increase of the density of the active particles, $N_{inv} \sim N \sim p$, and the intensity is sufficient to excite the molecules over the entire length of the active medium.

If the pump is monochromatic* ($\delta\nu_p << \Delta\nu_p^D$), this leads to "hole burning" in the Doppler-broadened absorption line. Dependence of the gain γ on the pressure and intensity of the pump is shown in Fig. 42 by the dashed lines. At $p << p_1$ and $I_p << I_{p0}$ the effect of "hole burning" leads to a narrowing of the emission line $\Delta\nu_l$, since the scatter of the velocities of the excited particles is much less in this case. This means that the gain will be larger than in the case of broadband pumping of the same intensity.

It should be noted, however, that the velocity scatter will increase with broadening of the "hole" and with increasing pump intensity. At $p < p_1$ and $I_1 < I_{p0}$ the "hole" burning effect limits the number of particles that can be excited compared with the case of broadband pumping, but still does not lead to a narrowing of the laser-transition line. In this case the gain will be already less than in broadband pumping of the same intensity. At $I_p >> I_{p0}$ single-frequency (monochromatic) pumping yields practically the same gain as broadband pumping, owing to the large field broadening of the "hole".

At nonresonant pumping, the maximum gain (dash-dot curves in Fig. 42) is less than at resonant pumping. However, if the pump intensity I_p is large enough for the broadening on account of saturation to become comparable with $\delta\nu_p^d = \nu_p - \nu_{13}$, the gain is the same as at resonant excitation. As seen from Fig. 42, if the value of I_p relative to I_{p0} is not known beforehand, the optimum pressure must be chosen to be $p \sim p_1$. If, however, it is known that $I_p << I_{p0}$, the optimum pressure region is $p < p_1$.

Chapter II. NONRESONANT COHERENT-RADIATION CONVERTERS — RAMAN LASERS

1. SRS as the Method of Effective Conversion of Laser Radiation

Stimulated Raman scattering of light (SRS) was discovered in 1962 [54], and interest in this form of frequency conversion of laser radiation has not abated to this day. By now several reviews have been published based on our earlier papers [55, 56, 57]. In the main they were devoted to the investigation of SRS on vibrational levels in the regimes of generation and amplification of an external signal in liquid nitrogen and in compressed hydrogen gas in the wavelength range 0.8–9 μm. These investigations have enabled us, in particular, to develop methods of exciting the active medium by using raster optics [58] that produce sources of coherent radiation operating in the heretofore unknown sections of the spectral band, some of which (see, e.g., [57]) are already used as laboratory instruments. We present below the results of investigations aimed at developing Raman lasers in a wider spectral band (0.3–16 μm), using new pump sources [59], new systems for the excitation of the active medium [60], and a shorter range of pulse durations $\tau \sim 3$ nsec [61]. The last paper [61] reports successful realization, for the first time with a high energy efficiency of 70%, of the idea of effective coherent summation [6] of a set of spatially separated pump beams into one beam of the Stokes component on the basis of SRS on rotational levels in H_2 gas.

By now there were developed on the basis of SRS many high-power sources of coherent radiation operating in new spectral bands. In accordance with their basic properties they can be regarded as an independent class of so-called Raman lasers.

As already noted many times, this class of lasers makes it possible to extend significantly the capabilities and consequently also the fields of application of the existing high-power optical lasers. Indeed, Raman lasers as frequency converters are in many cases

*In practice it is difficult to realize such a case, for this calls for the use of a single-mode and single-frequency pump source. For example, for molecular ammonia (M = 17, T = 300 K) pumped by a CO_2 laser with $\nu_p = 10^3$ cm^{-1} we have, in accordance with (21), $\delta\nu_p << \Delta\nu_p^D = 1.2$ MHz.

the only sources of high-power coherent radiation in individual sections of the spectral band. The advantage of such frequency converters lies in the fact that the nonresonant method of exciting the active medium ensures conversion of the initial laser radiation in a large number of media with different frequency shifts of the Stokes components. In this case several Stokes components can be generated simultaneously [56] or else (under certain conditions) one prescribed component can be generated [57]. In addition, this nonresonant form of excitation admits of the possibility of conversion, in one and the same medium, of radiation from various pump sources that are tunable in frequency. The combination of both properties makes it possible to operate in practically the entire wavelength range from 0.3 to 20 μm. Thus, e.g., in [59, 62] there were obtained series of lines in the UV and visible bands; in [63, 64] radiation with continuous frequency tuning from 0.72 to 7.7 and from 0.7 to 7 μm, respectively, was obtained; operation at 8.3–9.1 μm was obtained in [57] and in the 16-μm region in [60, 65, 66].

Another important property of Raman lasers is that they make it possible to substantially improve the quality of the laser radiation, namely to increase the energy density, power, and intensity, to decrease the beam divergence, and, what is most important for practical applications, to effect summation of energies from a large number of pump beams into a single Stokes-component light beam with high efficiency and with increased radiation brightness [61].

In addition, SRS lasers make it possible to shape light pulses with steep leading edges [55] and to either increase [67] or decrease [55, 58] the pulse duration. Unfortunately, these properties of Raman lasers have not yet been sufficiently well investigated and fully realized.

2. Active Media of Raman Lasers

It is difficult even to list all the media in which stimulated Raman scattering was investigated. These include compressed gases, organic liquids, and solids, as well as cryogenic liquids. Nonetheless, to develop high-power Raman lasers, out of all the abundance of active media, the most widely used in practice are compressed hydrogen and liquid nitrogen.

Hydrogen and liquid nitrogen (and their analogs deuterium and liquid oxygen) are in a certain sense unique media, most fully satisfying all the requirements imposed on active media of Raman lasers. Hydrogen is one of the few media in which SRS is the basic form of stimulated scattering. In hydrogen gas it is possible to have SRS both on vibrational levels [69] with a frequency shift $\nu_v = 4155\ cm^{-1}$, as well as on rotational levels [70]. The frequency shift in SRS on rotational transitions in H_2 depends on the particular hydrogen-molecule modification on which the Raman scattering takes place. It is known that the hydrogen molecule can be in one of two states, each of which is characterized by the relative orientation of the nuclear spin. If the spins are parallel (orthohydrogen), the rotational quantum number J can be only odd: J = 1, 3, ... If the spins are antiparallel (parahydrogen), J can be only even: J = 0, 2, ... Transitions between ortho and para states are parity forbidden, and ortho–para conversion is very slow. Therefore, Raman scattering is possible either in parahydrogen (the transition $J = 0 \rightarrow J = 2$, Stokes shift $\nu_v = 354\ cm^{-1}$) or in orthohydrogen ($\nu_v = 587\ cm^{-1}$, $J = 1 \rightarrow J = 3$) (Fig. 43).

Gaseous parahydrogen can be obtained and SRS can be observed in it at relatively high temperatures, $T \simeq 77°K$ and higher [71], by evaporating parahydrogen from a Dewar vessel. However, the time of existence of such a gas is limited to several hours, during which there is established an equilibrium concentration corresponding to Table 6, which lists the temperature dependences of the equilibrium relative population densities n_J of the level J = 0 in parahydrogen and of the level J = 1 in orthohydrogen.

The gain in SRS is proportional to n_J. Therefore, as seen from the table, SRS in parahydrogen with a partial shift $354\ cm^{-1}$ is possible only at low temperatures. At room temperature ($T \simeq 300$ K), in turn, orthohydrogen predominates. The greater part of the molecules are in a state J = 1 (the population of the J = 3 level can be neglected). Therefore, a Stokes shift $\nu_v = 586.85\ cm^{-1}$ is observed at room temperature, corresponding to the transition $J = 1 \rightarrow J = 3$.

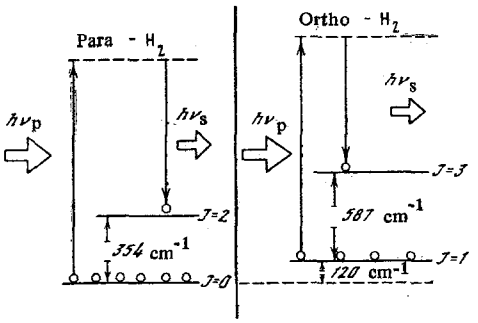

Fig. 43. SRS processes in parahydrogen and orthohydrogen.

TABLE 6

Temperature (deg K)	25	50	75	100	200	300
$n_{J=0}$ (parahydrogen; s (0); ν_V = =354,33 cm^{-1}; transition $J=0\rightarrow$ $\rightarrow J=2$)	0,992	0,788	0,535	0,388	0,193	0,133
$n_{J=1}$ (orthohydrogen; s (1); ν_V = =586,85 cm^{-1}; transition $J=1\rightarrow$ $\rightarrow J=3$)	0,008	0,211	0,462	0,603	0,719	0,667
$n_{J=0}$ (paradeuterium; s (0); ν_V = =179,04 cm^{-1}; transition $J=0\rightarrow$ $\rightarrow J=2$)	0,952	0,769	0,608	0,449	0,267	0,182
$n_{J=1}$ (orthodeuterium; s (1); ν_V= =297,52 cm^{-1}; transition $J=1\rightarrow$ $\rightarrow J=3$)	0,047	0,208	0,291	0,313	0,260	0,205
$n_{J=2}$ (paradeuterium; ν_V(2); ν_V= =414,71 cm^{-1}; transition $J=2\rightarrow$ $\rightarrow J=4$)	—	0,023	0,097	0,188	0,367	0,387

The maximum gain for SRS of a ruby laser (λ_p = 0.6943 μm) on vibrational levels is reached for a linearly polarized pump and amounts to g = 1.5 × 10^{-3} cm/MW [69] at a pressure p = 30–60 atm. For SRS on rotational levels at room temperature, the maximum value of the gain is g = $2\cdot10^{-3}$ cm/MW (λ_p = 1.06 μm) at a pressure p = 8 atm [72]. In this case the pump must be circularly polarized.

Liquid nitrogen is superior in a number of parameters compared to hydrogen gas. In particular, the gain in liquid nitrogen is approximately ten times larger than in H_2, and amounts to g = $1.6\cdot10^{-2}$ cm/MW (λ_p = 0.06943 μm) [73]. The optical-breakdown strength is likewise larger by almost an order of magnitude than for hydrogen gas. The frequency shift of SRS on vibrational levels in liquid N_2 amounts to ν_v = 2326 cm^{-1}. To be sure, if the pump pulse duration $\tau \gtrsim$ 500 nsec and the spectral line width $\delta\nu$ = 0.03 cm^{-1}, other types of stimulated scattering compete with SRS: stimulated temperature scattering (STS) and stimulated Brillouin scattering (SBS) [74]. This imposes definite limitations on the pump when working with liquid nitrogen. In addition, as shown by us in [57], the development of Raman lasers using cryogenic liquids calls for the solution of a number of technological problems connected with attaining a high optical homogeneity and transparency of these media.

3. Methods of Exciting Raman Lasers

The method of exciting a chosen active medium is determined principally by the capabilities of the pump source and primarily by such pump parameters as the power, divergence, wavelength, and initial beam diameter, and the method itself determines in turn the limiting characteristics of the converted radiation.

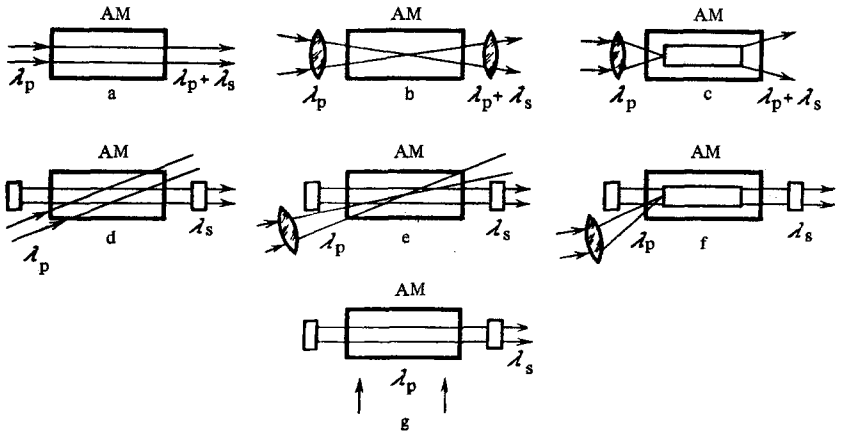

Fig. 44. Schemes of longitudinal excitation of an active medium: a, d) with a parallel beam; b, e) with the aid of a lens; c, f) lenses in conjunction with a light pipe; g) transverse variant.

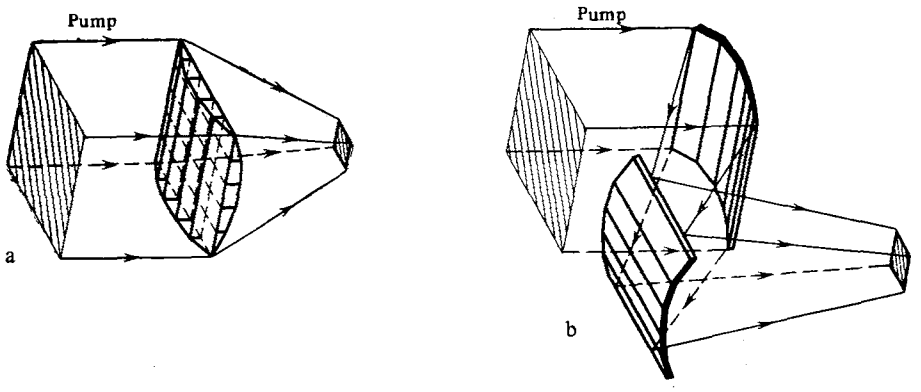

Fig. 45. Raster focusing systems.

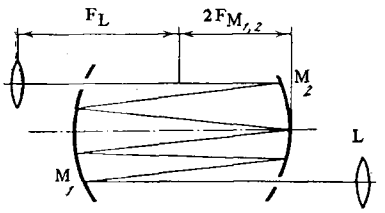

Fig. 46. Multipass focusing system.

Let us recall some of the features of known excitation methods (Fig. 44).

The simplest scheme of frequency conversion on the basis of SRS is shown in Fig. 44a. In this scheme the Stokes radiation is generated as a result of one pass of the parallel pump beam through the active medium (AM). The gain increment, which should amount in this case to approximately 30, is determined by the expression*: $b = g(4P/\pi D^2)L$, where g is the gain (in cm/MW); P, pump power (in MW); D, pump-beam diameter (in cm). Naturally, such a system makes it possible only to vary the frequency of the laser radiation without improving any of its characteristics. Despite its simplicity, it is extremely rarely used, for it calls for highly intense exciting radiation, and, in addition, the divergence of the converted radiation can be much worse than that of the pump.

*The expressions given here and below for b make it possible only to estimate the gain growth rate, since no account is taken in them of the intensity distribution over the beam cross section.

The most widely used is the scheme of frequency conversion shown in Fig. 44b, in which the pump is focused by a lens having a focal length F = L/2 into the center of the cell with the active medium. The maximum gain is reached in this case when the lens is in the plane of the cell window, and the gain growth rate can be estimated with sufficient accuracy from the formula $b = g(4P/\pi D d_f)$ [57] (where d_f is the diameter of the focal spot). In this case, compared with the preceding scheme and other conditions being equal, the pump power required for frequency conversion is smaller by approximately the same factor by which the beam diameter at the entrance to the cell exceeds the focal spot. The divergence of the Stokes components is usually equal to the pump divergence.

The system with the smallest threshold intensity of the exciting radiation, which ensures effective conversion of the pump in one pass through the active medium, is shown in Fig. 44c. Here the pump-source radiation is focused on the end face of the light pipe, whose length (if the losses in it are small) determines the minimum value of the power needed for frequency conversion.

The described method of excitation of the active medium can also be used in the development of Raman lasers and amplifiers (Figs. 44d, e, f).

Frequency conversion on the basis of SRS with the aid of Raman lasers differs qualitatively from conversion in accord with the single-pass scheme. The presence of a cavity makes it possible in this case to also utilize one of the most important properties of laser systems, namely, to concentrate the radiation in a narrow solid angle. Even in the case of conversion with high efficiency, the radiation brightness of the Raman laser can in this case exceed the pump brightness by hundreds of times [75].

Figure 44g shows a Raman laser with transverse pumping. In this system the exciting radiation propagates perpendicular to the optical axis of the cavity. This excitation method offers great possibilities from the energy point of view. For a number of reasons, however, particularly because of the difficulty of constructing the optical cells (e.g., cryogenic or high-pressure) that ensure high optical homogeneity of the active medium, this method has not found wide use. Thus, e.g., there is only one paper devoted to the investigation of a Raman liquid-nitrogen laser with transverse pumping [76].

The described methods of exciting Raman lasers using a lens, or a lens combined with a light pipe of round cross section, suffer from a substantial shortcoming. Owing to optical breakdown of the active medium (in gases) or to violation of the optical homogeneity (in liquids [57]) in the focal plane of the lens, these pumping methods ensure reliable operation only at energies not exceeding several dozen joules for pulse durations $\tau \sim 30$ nsec.

A qualitatively new method developed by us, which practically eliminates the energy limit, consists of replacing the lens by a raster (Fig. 45) [58]. The raster does not focus the radiation, but breaks it up into a large number of parallel beams of square cross section and gathers them at one and the same place in a given focal plane. Usually the raster takes the form of two crossed sets of glass wedges (Fig. 45a). To decrease the losses due to reflections from the surfaces, the raster can be made of two crossed sets of adjustable rectangular mirrors (Fig. 45b). Such a construction is convenient, because it makes it possible to vary the focal length of the raster. The number of adjustable mirrors is smaller by a factor k/2 than the number of beams into which the initial radiation is broken up (k is the number of mirrors in one set).

The combination of a raster with a light pipe of square cross section makes it possible to obtain a spatially uniform excitation of the active medium along the entire length of the light pipe [57]. In individual cases, the square light pipe can be replaced, to simplify the construction of the Raman laser, by a round light pipe (glass tube) [60].

All the schemes considered above for frequency conversion in gaseous H_2 and in liquid N_2 were successfully used in studies aimed at the development of Raman lasers for the ultraviolet, visible, and near infrared bands, up to 9 μm. This wavelength of such Raman lasers has turned out to be the limit at present. The point is that both the gain for SRS and the optical breakdown strength of the active medium decrease with increasing wavelength [77]. Also decreasing is the value of the threshold intensity of the light, which leads to surface breakdown of dielectrics and metals, so that a light pipe cannot be used. As a result, and with allowance for the fact that the gain growth rate $b = gI_pL$ increases linearly both as a function of the pump intensity and as a function of frequency, it is necessary, at a fixed

value of I_p, determined by the optical breakdown strength of the active medium, to increase its length. In this case, since $b=gI_pL=g\,(4P_p/\pi d\,(d+\Theta L)\,L$ (for the scheme of Fig. 44a), it is necessary to take into account the fact that the gain growth rate will increase linearly with increasing length of the active medium only if the condition $\Theta L \ll d$ is satisfied. Estimates show that for the diffraction divergence of the pump radiation (i.e., $\Theta \simeq 2{,}44\,\lambda/d$) with wavelength λ_p = 10 μm (CO_2 laser) the left-hand side of this inequality will amount to one-tenth of the right-hand side at L = 40 cm. This means that to obtain a gain growth rate of 30 over such a length the pump intensity required is $I_p \simeq 10^4$ MW/cm^2. This greatly exceeds also the limiting intensity determined by the optical breakdown strength of both the cell windows and the active medium.

The scheme shown in Fig. 44b, where the pump is focused into the center of the cell with active medium, can likewise not be used, for in this case the growth rate b depends little on the length of the active medium and is determined only by the power and divergence of the pump radiation and by the light-beam diameter.

Figure 46 shows a multipass system which was used in practically all the developments of a source of coherent radiation based on SRS in the wavelength region ∿16 μm [60, 65, 66]. In this case the pump radiation is focused into the center of curvature of one of the mirrors, which are spaced 4F apart. It is then possible to use either two spherical mirrors [66], or two sets of independently adjustable mirrors [60]. The second variant is technically more complicated, but it makes it possible, if necessary, to use mirrors with different focal lengths, so that the number of passes can be decreased. Indeed, as the pump is being converted into the Stokes component the radiation intensity decreases because of the Stokes losses, and if a liquid medium such as N_2 is used, it decreases also because of scattering of the light. These losses are larger the shorter the wavelength of the initial radiation. It is possible to maintain the value of the focal intensity within limits determined by the optical breakdown strength of the medium at the expense of decreasing the focal distance of the mirrors with increasing number of passes.

Thus, a multipass optical system makes it possible to choose the required value of the growth rate b for effective conversion of the pump into the Stokes component. The value of b per pass is determined here by the optical breakdown strength of the medium, and the number of passes is determined by the gain for SRS.

4. Raman Laser for the Near-Ultraviolet and for the Visible Band

Promising sources of laser radiation for the near ultraviolet are excimer lasers [79], which are already being used to solve many physical problems. The range of their applicability can be greatly expanded by improving the divergence of the radiation, by shortening the pulse duration, and by attaining frequency tuning in the visible band. In principle, these problems can be solved by converting the laser radiation on the basis of SRS, and the first attempts in this direction were undertaken in [59, 68, 78].

The experimental setup of [59] is shown in Fig. 47. The pump source was an electric-discharge laser (EL) operating on transitions of the XeF molecules in the mixture NF_3:Xe:He = 1:3:500, and of XeCl in the mixture HCl:Xe:He = 1:15:500 with total pressure 1.5-2.5 atm [80]. The main characteristics of the laser radiation were the following: energy E_p = 0.1–0.5 J, divergence $\Theta_p = 10^{-2}$ rad, pulse duration at half intensity τ_p = 25 nsec. The pump radiation was focussed with a lens L_1 having a focal length F_1 = 40 cm into the center of a cell L = 50 cm long, filled with liquid nitrogen. Part of the pump energy was diverted with a plane-parallel plate (P) of CaF_2 into a calorimeter (K_1). The emission of the Stokes components and of the nonconverted pump was directed with the aid of lens L_2 (F = 30 cm) through a dispersion system consisting of three quartz prisms (Pr) into the calorimeters K_2–K_4. Thus, in each experiment there were registered the energy characteristics of the pump at the entry to the cell (K_1) and at its exit (K_3), and of the following Stokes components: the first with wavelength λ_{S1}(K_4), and the second with wavelength λ_{S2}(K_2). In a number of cases at $E_p \simeq 140...160$ mJ a third Stokes component was observed in the spectrum of the converted radiation. Its energy, however, was low and therefore was not measured

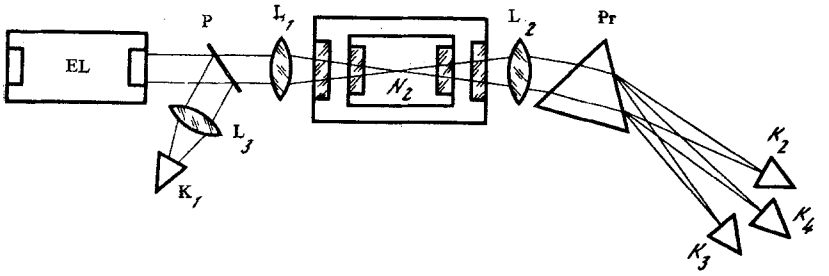

Fig. 47. Block diagram of setup intended for the investigation of a liquid-nitrogen Raman laser pumped by XeF and XeCl lasers.

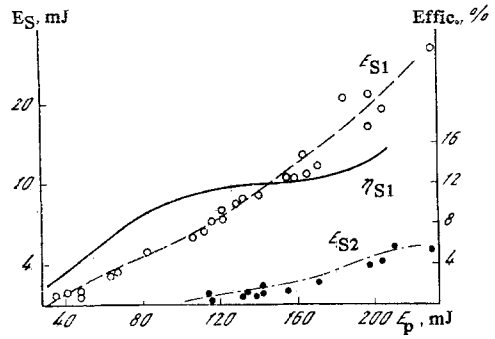

Fig. 48

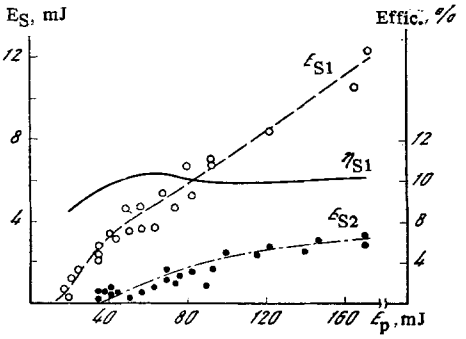

Fig. 49

Fig. 48. Energy characteristics of a liquid nitrogen Raman laser pumped by an XeF laser; λ_p = 351 nm, λ_{S_1} = 382 nm, λ_{S_2} = 420 nm.

Fig. 49. Energy characteristics of a liquid-nitrogen Raman laser pumped by an XeCl laser; λ_p = 308 nm, λ_{S_1} = 332 nm, λ_{S_2} = 359 nm.

Figures 48, 49 show plots of the energies of the first (E_{S_1}) and second (E_{S_2}) Stokes components, and also the efficiency of conversion into the first Stokes component η_{S_1} against the pump energy. It can be seen that the maximum values of the radiation energy of both the first and second Stokes components are reached at maximum pump values. The conversion efficiency flattens out because of the onset of the second Stokes component, which limits the growth of the first. A subsequent increase of η_{S_1} is observed when the third Stokes component appears.

An electric-discharge laser can operate both in the monopulse and in the repeated-pulse (RP) regimes. Working in the repeated-pulse regime, a typical value of the energy of an individual pulse amounted to $E_p \simeq 100$ mJ. At this value of E_p (see Figs. 48, 49) the conversion efficiency was η_S = 8–10%, and this gave grounds for hoping to obtain a sufficiently high conversion efficiency when the Raman laser operates in the RP regime. Experiments have shown, however, that at a pump pulse repetition frequency $\nu \geq 1$ Hz the conversion efficiency η decreases practically to zero within a time $t \simeq 1$ min. The transparency of the liquid nitrogen here became much worse and was restored to the initial level after several hours.

The change in the transparency of the liquid nitrogen is due to the presence in it of suspended particles [57]. High-power pumping breaks up these particles into a set of smaller particles, and this leads to a strong increase of the scattering of the pump and of the Stokes component. A more thorough cleaning of the nitrogen to eliminate mechanical impurities will apparently make it possible to increase the transparency of the liquid active medium and will permit effective conversion of the pump in SRS in liquid nitrogen in the repeated-pulse regime.

5. Raman Laser Tunable in the 1.89-, 3.39-, and 16-μm Bands

The neodymium laser is at present one of the most widely used sources of coherent radiation. Many of its parameters are of record size even now. The frequency of its radiation

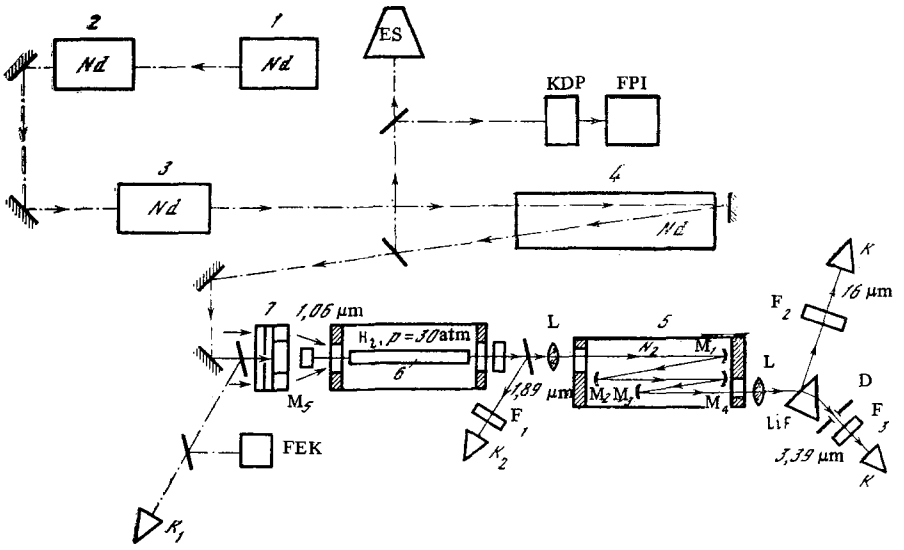

Fig. 50. Block diagram of setup intended for the investigation of the conversion of neodymium-laser radiation into the region 16 μm: 1) master oscillator; 2) Q-switched laser; 3, 4) amplifier; 5) cell; 6) light pipe; 7) raster; ES) echelette spectrograph; KDP) crystal; FPI) Fabry–Perot interferometer; FEK) coaxial photocell.

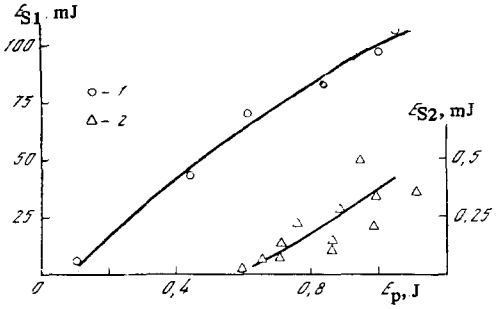

Fig. 51. Dependence of the first and second Stokes components of SRS in N_2 on the energy of the hydrogen generator — the pump source (λ_p = 1.89 μm). 1) λ_{S_1} = 3.39 μm; 2) λ_{S_2} = 16 μm.

can be smoothly tuned in a sufficiently wide range, and, depending on the experimental conditions, the laser can operate in the monopulse, pulse-train, or repetition regime. All these properties make the problem of developing Raman frequency-tunable lasers pumped by neodymium lasers urgent. One such study is described in [60].

We present below results of experiments on direct conversion, only on account of SRS, of the radiation of a Q-switched neodymium laser into the wavelength regions 1.89, 3.39, and 16 μm.

The neodymium laser, whose arrangement is similar to that described in [81], consisted of a master oscillator tunable in frequency and working in the free-lasing regime, a controllable Q-switched laser, and two amplifiers (Fig. 50). Its parameters were the following: energy E_p = 35 J, pulse duration τ_p = 50 nsec, divergence $\Theta_p = 3 \times 10^{-3}$ rad, spectrum width $\Delta\nu_p$ = 0.05 cm^{-1}. It must be noted that optical decoupling devices used in [81] were not used in the present system. This has made it possible to achieve a high radiation power P_p = 0.7 GW with a smaller number of amplification stages. However, at the maximum energy output E_p = 35 J the laser was excited, and this led to a substantial broadening of the spectrum and to a decrease of the radiation power.

The Raman laser with hydrogen compressed to 30 atm as the medium consisted of a high-pressure chamber placed in a cavity, in which the light pipe was placed. The light pipe was a glass tube of 10 mm diameter and 800 mm length, making the construction of the laser simpler than that investigated in [81]. The minimum diameter was determined, in particular, by the threshold pump energy at which a spark was produced in the round light pipe.

The hydrogen Raman laser was pumped with a raster [58] with cell dimensions 0.5 × 0.5 cm and focal length F_r = 40 cm. This excluded the possibility of a spark breakdown in the active medium at the entrance to the light pipe.

The maximum energy of the first Stokes component with wavelength λ_S = 1.89 μm amounted to $E_S^{H_2}$ = 2 J at a conversion efficiency up to 15%. The divergence at half-intensity level was 2—3 times smaller than that of the pump, and amounted to $(1...1.5)\cdot10^{-3}$ rad.

The conversion of the hydrogen-laser radiation into the farther infrared band was effected in a cryogenic cell L = 50 cm long filled with liquid nitrogen. The optical system of the conversion is a multipass focusing system (M_1—M_4) located in the working volume of the cell. The curvature radii of the employed gold-coated copper mirrors were 500 mm (M_1, M_2) and 80 mm (M_3, M_4).

The pump (λ_p = 1.89 μm) was focused in the focal plane of mirror M_1. The radiation converted in the N_2 on the first (λS_1 = 3.39 μm) and second (λS_2 = 16 μm) components was separated with the aid of an LiF prism and was recorded with calorimeters. The energy of the first Stokes component reached E_{S_1} = 100 mJ, and that of the second E_{S_2} = 0.5 mJ (Fig. 51).

Since the parameters of the optical systems were not optimized, the energies obtained in all three bands are far from the limit. It was established that even after the first passage of radiation with wavelength λ_S = 1.89 μm through the liquid nitrogen, a strong scattering, due to the high intensity of the light, is observed. This lowered the conversion efficiency and did not make possible full use of the advantages of the multipass scheme. Nonetheless, the efficiency of conversion, in N_2, into the first Stokes component at a pump energy 1 J amounted to 10%, thereby ensuring the necessary excess above the threshold intensity for further conversion of radiation into the second Stokes component.

6. Hydrogen Raman Laser on Rotational Transitions for Effective Coherent Summation of Nanosecond Light Pulses

Modern laser installations, intended, e.g., for thermonuclear fusion, must meet exceedingly stringent requirements, satisfaction of which, if the installation is constructed in accordance with the traditional laser—amplifier scheme, is a highly complicated matter.

In [6] is presented one of the new ways of solving this problem, and its main idea consists of using the initial multichannel laser setup as a source for pumping Raman lasers (Fig. 52), and concentrating the converted radiation on the target. In this case the requirements imposed on the pump source are substantially relaxed. The source must ensure the specified energy and the power necessary for the SRS at a sufficiently large divergence ($(0.5—1)\times10^{-2}$ rad). The small divergence and the high energy density are achieved by frequency conversion of the pump in the Raman laser. The advantage of such a scheme over the traditional one is obvious. The use of high-efficiency Raman lasers as the output stages of a multichannel facility can not only increase the brightness of the laser radiation, and exclude the possibility of self-excitation of the facility on account of reflection of the radiation from the target, but also decrease (by tens and hundreds of times) the number of light beams whose energy must be concentrated on the target.

Reference [61] is devoted to the development and investigation of a Raman laser for effective coherent summation of a large number of light beams from a neodymium laser operating in the range of nanosecond pulses.

The term "coherent summation" means that as a result of the nonlinear interaction of the medium with laser radiation, n pump beams, each of which has a cross section S_p, are converted into one spatially coherent beam of the Raman laser with cross section S_c, in

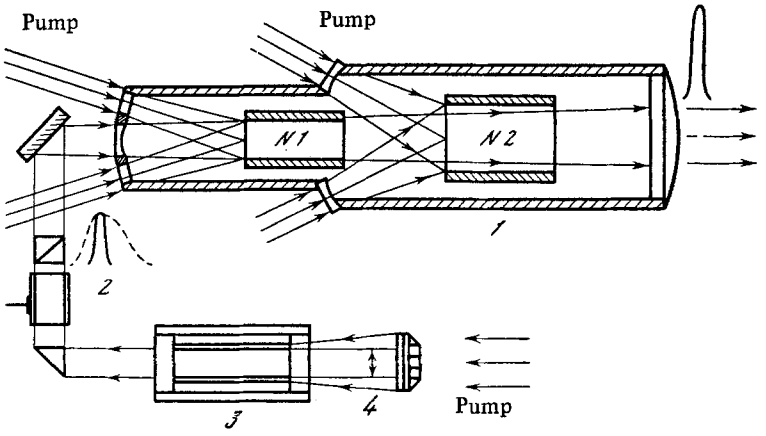

Fig. 52. Multistage Raman converter of laser radiation: 1) light pipe; 2) optical shutter; 3) laser; 4) raster.

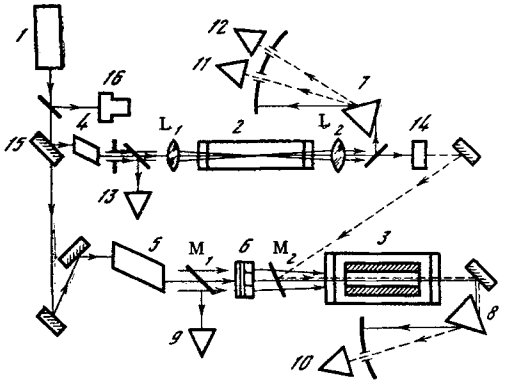

Fig. 53. Block diagram of setup for the measurement of the gain of the SRS radiation of a neodymium laser on rotational levels in hydrogen gas: 1) pump source — neodymium laser; 2) converter; 3) Raman amplifier; 4, 5) Fresnel parallelepipeds; 6–16) recording apparatus.

which the energy density is $n\eta(S_p/S_c)$ times larger than in the pump (η is the conversion efficiency).

The choice of hydrogen gas as the active medium was based on preliminary experiments on the investigation of Raman scattering on rotational levels in gaseous hydrogen with a frequency shift $\nu_{exc}^{H_2} = 587$ cm^{-1} [72].

A block diagram of the experimental setup used for the investigations and for the measurement of the gain and of its dependence on the pressure is shown in Fig. 53. The setup consisted of a neodymium laser (the pump source), a converter, a Raman amplifier, and a recording apparatus. The $\lambda/4$ plates were Fresnel parallelepipeds.

A neodymium laser Q-switched by a passive shutter emitted linearly polarized light pulses of energy $E_L = 0.7$ J and pulse duration $\tau = 12$ nsec at half-intensity level. The diameter of the light beam was 1 cm, and its divergence amounted to $\theta = 1.5 \cdot 10^{-3}$ rad. The width of the lasing spectrum was $\Delta\nu_L \leqslant 0.05$ cm^{-1}. Part of the pump energy was diverted with a dielectric mirror and focused by a lens of focal length F = 60 cm in the center of the 1-m converter cell filled with hydrogen gas. The converted radiation (the first Stokes SRS component, $\lambda_S = 1.13$ μm) was directed into a square light pipe of length L = 70 cm and cross section 0.5 × 0.5 cm placed inside the Raman-amplifier cell. The cells of the Raman amplifier

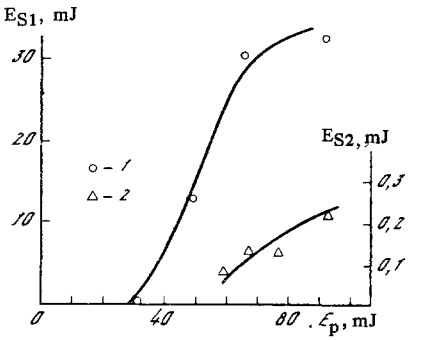

Fig. 54

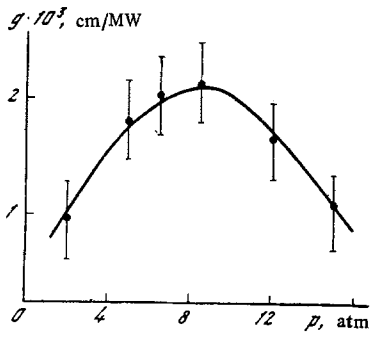

Fig. 55

Fig. 54. Dependence of the energies of the first and second Stokes components on the pump energy (λ_p = 1.06 μm): 1) λ_{S_1} = 1.13 μm; 2) λ_{S_2} = 1.21 μm.

Fig. 55. Dependence of the SRS gain on the hydrogen pressure for opposite directions of rotation of the circular polarizations of the Stokes signal and of the pump.

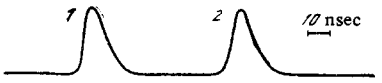

Fig. 56. Pulse of Stokes signal (1) and of pump (2) at the input of a Raman amplifier.

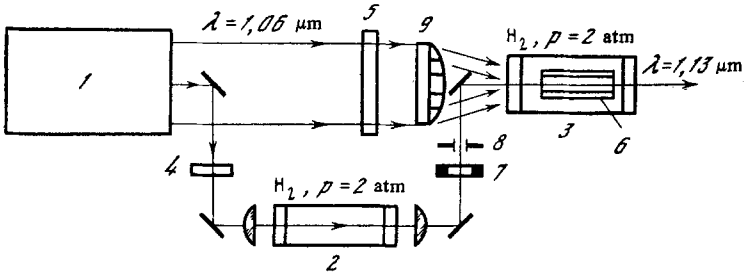

Fig. 57. Diagram of setup intended for research into the effective coherent summation of nanosecond light pulses in compressed H_2: 1) neodymium laser (pump source); 2) cell 1-m long filled with hydrogen (p = 2 atm); 3) Raman amplifier (cell filled with hydrogen, p = 2 atm); 4, 5) λ/4 plates — Fresnel parallelepipeds; 6) light pipe with cross section 0.5 × 0.5 cm and length 50 cm; 7) interference filter (E_{S_2}/E_{S_1} = 1/100); 8) diaphragm 0.5 × 0.5 cm; 9) raster.

and of the converter were joined by a tube in order to maintain equal hydrogen pressures in them. The amplifier was pumped with a raster with cell dimension 0.5 × 0.5 cm, thus ensuring uniform illumination of the light pipe over the entire length.

Figure 54 shows the dependence of the energy of the first (λ_{S_2} = 1.13 μm) and second (λ_{S_1} = 1.21 μm) Stokes components on the converter pump energy. It can be seen that the maximum efficiency of the conversion into the first Stokes component is close to 50%, and in this case there is practically no second Stokes component. This efficiency value is reached at a pump energy E_p = 60–80 mJ. Its further increase led to optical breakdown in the active medium, thereby substantially decreasing the conversion efficiency.

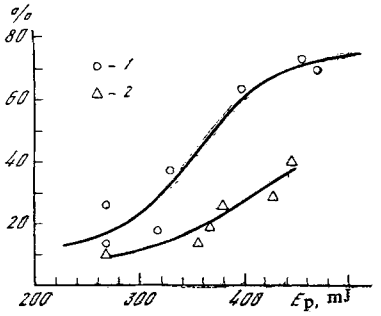

Fig. 58. Energy results of coherent summation of 50 pump beams in the amplification regime: 1) E_{in} = 12 mJ; 2) E_{in} = 5 mJ.

Figure 55 shows the dependence of the gain on the hydrogen pressure for the case when the pump and the output signal were circularly polarized with opposite directions of rotation. The maximum value $g_{\circlearrowleft}=(2{,}0\pm0{,}4)\cdot10^{-3}$ cm/mW was assumed by the gain at a hydrogen pressure p_{opt} = 8 atm. In its calculation the pump and output-signal pulses were approximated by triangles, in agreement with the true shape (Fig. 56).

In the case when the polarizations of the exciting and Stokes radiations rotated in the same direction, the gain at optimal pressure p_{opt} = 8 atm decreased to a value $g_{\circlearrowright}=(4\pm1)\cdot10^{-4}$ cm/mW. These results agree well with the theoretical conclusions of [70]. The measured value of the gain and the value of the gain for SRS on vibrational levels (g_V = 1.5 × 10^{-3} cm/mW) turned out to be very close, in agreement with the real conditions. Thus, when using a converter in the form of a cell 3 m long (p = 10 atm), the output radiation contained the first SRS Stokes components both on the vibrational and on the rotational levels. In addition, it was observed that the efficiency of conversion into only one first Stokes component on the basis of SRS on rotational levels in hydrogen gas, without any special measures to suppress the second Stokes component, can reach the appreciable value $\eta \simeq 50\%$. By way of comparison one can note that the efficiency of conversion in liquid nitrogen in a similar scheme does not exceed 20%. Even at this value, lasing takes place on the second Stokes component, thereby lowering the efficiency of conversion into the first. This gave grounds for hoping that SRS on rotational levels in hydrogen, in accordance with the generator–amplifier scheme, can be used to develop a laser-radiation summator of high energy efficiency.

The range of pump-pulse durations determined the scheme of the Raman laser–summator that should operate in the regime of saturated amplification of the external signal.

A simplified diagram of the experimental setup is shown in Fig. 57. It contains the pump source – a neodymium laser consisting of a master oscillator, electrooptical shutter, preamplifier, and recording apparatus. Rotation of the pump polarization was effected with Fresnel parallelepipeds. The master oscillator operated in the Q-switched regime with a passive shutter and emitted light pulses with a linear polarization and with duration $\tau_p \simeq 30$ nsec. The electrooptical shutter was used to shape a pulse of duration τ_p = 3 nsec. The preamplifier and amplifier operated in accordance with a two-phase scheme. The parameters of the output radiation of the neodymium laser were the following: energy E_p = 1.5 J; pulse duration τ_p = 3 nsec; divergence at half the energy level θ_p = 3 × 10^{-3} rad, spectral width $\Delta\nu_p \leqslant 0.05$ cm^{-1}.

The Raman laser – the source of the input signal – was cell of length L = 1 m filled with hydrogen at pressure up to 2–8 atm. The Raman amplifier was constructed in the form of a cell 70 cm long, inside of which was placed a 50-cm light pipe with cross section 0.5 × 0.5 cm. The length of the light pipe was determined in this case by the value of the gain g and by the chosen value of the pump intensity $I_p \sim 1$ GW/cm², while its cross section was determined by the value of the output signal. For effective conversion, the intensity of the

TABLE 7

Characteristics	Pump source	H_2 Raman laser
Wavelength, μm	1,06	1,13
Number of beams	50	1
Beam cross section, mm	5×5	5×5
Pulse duration, nsec	3	3
Divergence θ, rad (at half the energy level)	$3 \cdot 10^{-3}$	10^{-3}
Energy, J	50×10^{-2}	0,36
Power, GW	$50 \times 0{,}33 \cdot 10^{-2}$	0,12
Energy density, J/cm^2	$4 \cdot 10^{-2}$	1,45
Intensity, GW/cm^2	$1{,}4 \cdot 10^{-2}$	0,48
Input-signal energy, J	—	$(12. . .14) \cdot 10^{-3}$
Brightness increase	—	300

input signal, according to [56], should amount to not less than 1% of the pump intensity, meaning that it should equal $I_{s,in} \simeq 10$ MW/cm. Since the input-signal source was a one-pass converter with focusing of the pump radiation into the active medium, with allowance for all the losses due to registration of the input signal parameters, filtration, and formation of the quadratic-cross-section beam to the light pipe, we were able to raise the energy to $E_{s,in} \simeq 10$ mJ. Consequently, the cross section of the light pipe should amount to $S \simeq 0.3$ cm^2.

Part of the pump energy was diverted with a mirror of 10 mm diameter and was focused into the laser cell by a lens of focal length F = 1 m. The output radiation of the laser passed through selective filters 7 that attenuated the second Stokes component by 100 times and through a diaphragm 8 with dimensions 0.5 × 0.5 cm, and was directed with the aid of a lens and two mirrors into the Raman-amplifier light pipe. The Raman amplifier was pumped with a raster using light beams of quadratic cross section with dimension 0.5 × 0.5 cm, each of which was fed to the end opening of a light pipe at a small angle to the optical axis. The number of such beams was 50, and the maximum energy contained in each of them was $E_{p.b.} =$ 10 mJ. Such a pumping of the Raman amplifier can be regarded as a model of a scheme for exciting a Raman laser using a large number of parallel output amplifiers of the pump source, operating from a single master oscillator.

In the case when the pressure in the cell was 8 atm, and the energy of the output signal with the frequency of the first Stokes component ν_S was 2—3% of the maximum value of the energy of all the pump beams ($E_p = 0.5$ J), the conversion efficiency in the amplifier reached 50%. In this case, however, almost 2/3 of the output-radiation energy was contained in the second Stokes component with frequency ν_{S_2}. Decreasing the intensity of the input signal improves this ratio in favor of the first Stokes component, but in this case the conversion efficiency increases. It was found possible to reduce to a minimum the energy output of the radiation at the frequency ν_{S_2} and its adverse influence on the conversion efficiency by decreasing the gain g. To this end, the pressure in the cells was lowered to 2 atm.

The results of these experiments are shown in Fig. 58. Accurate to the sensitivity of the calorimeter, which can register an energy of 5 mJ, the converted radiation does not contain the second Stokes component, and the maximum efficiency of conversion into the first reaches 70%. The shape and duration of the pump pulses and of the converted radiation were practically the same.

The basic characteristics of the pump and of the converted radiation are given in Table 7.

Thus, in the present study we have realized for the first time ever, with high efficiency ($\eta = 70\%$), coherent summation of the energy of 50 beams from a neodymium laser operating in the nanosecond-pulse regime. The results suggest that the development and improvement of such Raman lasers will uncover possibilities for their use in laser facilities of the "Del'fin" type, intended to obtain laser thermonuclear fusion [6].

LITERATURE CITED

1. N. G. Basov, A. N. Oraevskii, and A. V. Pankratov, Chemical and Biochemical Applications of Lasers, Academic Press (1974), p. 207.
2. V. S. Letokhov and S. B. Mur, Kvantovaya Elektron. (Moscow), 3, 248, 485 (1976).
3. N. V. Karlov and A. M. Prokhorov, Usp. Fiz. Nauk, 118, 583 (1976).
4. N. G. Basov, É. M. Belenov, V. A. Isakov, E. P. Markin, A. N. Oraevskii, and V. I. Romanenko, Usp. Fiz. Nauk, 121, 427 (1977).
5. V. S. Letokhov and V. P. Chebotarev, Principles of Nonlinear Laser Spectroscopy [in Russian], Nauka, Moscow (1975).
6. N. G. Basov, "Principles of high-power laser constructions for controlled thermonuclear fusion," P. N. Lebedev Physical Institute, Moscow, Preprint No. 153 (1978).
7. N. G. Basov, A. Z. Grasyuk, and V. A. Katulin, Dokl. Akad. Nauk SSSR, 161, 1306 (1965).
8. N. G. Basov, A. Z. Grasiuk, V. E. Efimkov, et al., J. Phys. Soc. Jpn., 21 (Suppl.), 277 (1966).
9. G. Magyar, "Dye-laser — a classified bibliography: 1966-1972," App. Phys., 13, 25, (1974).
10. T. Y. Chang and D. R. Wood, Appl. Phys. Lett., 21, 19 (1972).
11. N. Scribanowitz, I. P. Hermann and M. S. Feld, Appl. Phys. Lett., 21, 466 (1972).
12. A. G. Golger and V. S. Letokhov, Kvantovaya Elektron. (Moscow), No. 1 (13), 20 (1973).
13. T. Y. Chang, in: Nonlinear Infrared Generation: Topics in Appl. Phys, ed. Shen, Berlin, etc. Springer-Verlag, 16, p. 215.
14. C. R. Jones, Laser Focus, 14, 68 (1978).
15. N. G. Basov and A. M. Prokhorov, Zh. Eksp. Teor. Fiz., 29, 249 (1955).
16. T. Y. Chang and J. D. McGee, Appl. Phys. Lett., 28, 526 (1976).
17. E. J. D. Lemicz, E. G. Malk, and P. D. Coleman, Appl. Phys. Lett., 29, 557 (1976).
18. T. Y. Chang and J. D. McGee, Appl. Phys. Lett., 29, 320 (1976).
19. S. M. Fray, Opt. Commun., 19, 320 (1976).
20. P. G. Harrison and F. A. Al-Watban, Opt. Commun., 20, 225 (1977).
21. B. Walker et al., Opt. Commun., 23, 8 (1977).
22. R. R. Jacobs et al., Appl. Phys. Lett., 29, 710 (1976).
23. W. K. Bischel et al., J. Appl. Phys., 49, 976 (1978).
24. J. J. Tee and C. Wittig, J. Appl. Phys., 49, No. 1, 61 (1978).
25. T. Moshizuki, M. Yamanaka, M. Marikawa, and C. Yamanaka, J. Opt. Soc. Am., 68, 672 (1978).
26. E. D. Shaw and G. K. N. Patel, Opt. Commun., 27, No. 3, 419 (1978).
27. B. I. Vasil'ev, A. Z. Grasyuk, and A. P. Dyad'kin, Kvantovaya Elektron. (Moscow), 4, No. 8 (1977).
28. B. I. Vasil'ev, A. P. Dyad'kin, N. P. Furzikov, and A. B. Yastrebkov, Pis'ma Zh. Tekh. Fiz., No. 7 (1979).
29. B. I. Vasil'ev, A. Z. Grasyuk, et al., Kvantovaya Elektron. (Moscow), No. 3 (1979).
30. B. I. Vasil'ev, A. Z. Grasyuk, A. P. Dyad'kin, and N. P. Furzikov, Krat. Soobshch. Fiz., FIAN, No. 2 (1978).
31. V. Yu. Baranov et al., Appl. Phys. Lett., 17, 317 (1978).
32. B. I. Vasil'ev, A. Z. Grasyuk, A. P. Dyad'kin, A. N. Sukhanov, and A. B. Yastrebkov, Kvantovaya Elektron. (Moscow), 7, No. 1, 116 (1980).
33. C. H. Townes and A. L. Schawlow, Microwave Spectroscopy, McGraw-Hill (1955).
34. A. L. Golger and V. S. Letokhov, Kvantovaya Elektron. (Moscow), No. 5 (17) (1973).
35. P. M. Valov, K. V. Goncharenko, Yu. V. Markov, V. V. Pershin, S. M. Ryvkin, and I. D. Yaroshetskii, Kvantovaya Elektron. (Moscow), 4, 95 (1977).
36. P. M. Valov, B. I. Vasil'ev, A. P. Dyad'kin, and A. P. Yaroshetskii, Fiz. Tekh. Poluprovodn., 12, 1288-1292 (1976).
37. J. J. Tee and C. Wittig, Appl. Phys. Lett., 30, 420 (1977).
38. B. I. Vasil'ev, A. Z. Grasyuk, A. P. Dyad'kin, and N. P. Furzikov, FIAN Preprint No. 26, Moscow (1978).
39. S. S. Alimpiev, G. S. Baranov, N. V. Karlov, et al., Pis'ma Zh. Tekh. Fiz., 4, 167 (1978).
40. Yu. A. Gorokhov, S. V. Efimovskii, I. N. Knyazev, and V. V. Lobko, Preprint ISAN, Moscow (1979).
41. Yu. R. Kolomiiskii, V. S. Letokhov, and O. A. Tumanov, Kvantovaya Elektron. (Moscow), 3, 1771 (1976).
42. V. S. Letokhov, A. A. Makarov, and E. A. Ryabov, Dokl. Akad. Nauk SSSR, 212, 75 (1973).

43. V. Yu. Baranov, B. I. Vasil'ev, E. P. Velikhov, et al., Kvantovaya Elektron. (Moscow), 5, 940 (1978).
44. R. V. Ambartzumian et al., Appl. Phys., 15, 27 (1978).
45. R. V. Ambartzumian et al., Phys. Lett., 56A, 183 (1976).
46. R. V. Ambartzumian et al., in: Chemical and Biochemical Applications of Lasers, Academic Press, Vol. 3 (1977).
47. A. P. Peterson et al., Opt. Commun., 17, 259 (1978).
48. R. V. Ambartzumian et al., Opt. Commun., 18, 517 (1976).
49. B. I. Vasil'ev, N. A. Vishnyakov, V. T. Galochkin, et al., Pis'ma Zh. Eksp. Teor. Fiz., 30, 29 (1979).
50. R. V. Ambartsumyan, G. N. Makarov, and A. A. Puretskii, Pis'ma Zh. Eksp. Teor. Fiz., 28, 246 (1978).
51. B. I. Vasil'ev, A. N. Sukhanov, and A. P. Dyad'kin, Pisma Zh. Tekh. Fiz., No. 4, 311 (1980).
52. P. Rabinowitz et al., Opt. Commun., 27, No. 3, 381 (1978).
53. R. V. Ambartsumyan, V. A. Apatin, N. G. Basov, A. Z. Grasyuk, A. P. Dyad'kin, and N. P. Furzikov, Kvantovaya Elektron. (Moscow), 5, 632 (1978).
54. E. J. Woodbury and W. K. Ng, Proc. IRE, 50, 2367 (1962).
55. A. Z. Grasyuk, Kvantovaya Elektron. (Moscow), 1, No. 3, 485 (1974).
56. A. Z. Grasyuk, Tr. FIAN, 76, 75 (1974).
57. A. Z. Grasyuk, V. F. Efimov, I. G. Zubarev, A. V. Kotov, and V. G. Smirnov, Tr. FIAN, 91, 116 (1977).
58. A. Z. Grasyuk, V. F. Efimkov, and V. G. Smirnov, Prib. Tekh. Eksp., No. 1, 174 (1976).
59. V. A. Baranov, V. N. Borisov, A. Z. Grasyuk, et al., Pis'ma Zh. Tekh. Fiz., 4, No. 24, 1211 (1979).
60. A. Z. Grasyuk, Yu. I. Karev, L. L. Losev, and V. G. Smirnov, Pis'ma Zh. Tekh. Fiz., 4, No. 20, 1253 (1978).
61. N. G. Basov, A. Z. Grasyuk, Yu. I. Karev, L. L. Losev, and V. G. Smirnov, Kvantovaya Elektron.(Moscow), 6, No. 6, 1329 (1979).
62. T. R. Loree, R. C. Sze, and D. L. Barker, Appl. Phys. Lett., 31, No. 1, 37 (1977).
63. M. Bierry, R. Frey, and F. Pradere, Rev. Sci. Instrum., 48, No. 7, 733 (1977).
64. W. Hartig and W. Schmidt, Appl. Phys., 18, 235 (1979).
65. R. Frey et al., Opt. Commun., 22, 355 (1977).
66. A. Kaldor et al., Opt. Lett., 3, No. 4, 244 (1978).
67. A. Z. Grasyuk, I. G. Zubarev, and V. F. Mulikov, Krat. Soobshch. Fiz., FIAN, No. 2, 27 (1971).
68. J. R. Murray et al., Appl. Phys. Lett., 33, No. 5, 339 (1978).
69. R. W. Mink, E. E. Hagenlocker and W. G. Rado, Phys. Rev. Lett., 3, 181 (1963).
70. R. W. Mink, E. E. Hagenlocker and W. G. Rado, Phys. Rev. Lett., 17, No. 5, 229 (1966).
71. R. Byer, IEEE J. Quantum Electron., 11, 732 (1976).
72. Yu. I. Karev, L. L. Losev, and V. G. Smirnov, Kvantovaya Elektron. (Moscow), 6, No. 10, 2274 (1979).
73. A. H. Mcquillan et al., Phys. Rev., 180, 61 (1969).
74. M. G. Gangardt, A. Z. Grasyuk, and I. G. Zubarev, Kvantovaya Elektron. (Moscow), No. 6, 120 (1971).
75. A. Z. Grasyuk, V. F. Efimkov, I. G. Zubarev, V. I. Mishin, and V. G. Smirnov, Pis'ma Zh. Eksp. Teor. Fiz., 8, No. 9, 474 (1968).
76. V. V. Bogarov, M. G. Gangardt, A. Z. Grasyuk, V. G. Smirnov, and E. A. Yukov, FIAN Preprint No. 104, Moscow (1969).
77. Yu. P. Raizer, Laser-Induced Discharge Phenomena, Consultants Bureau (1977).
78. J. R. Murray, J. Goldner and A. Sroke, Appl. Phys. Lett., 32, 551 (1978).
79. N. G. Basov, V. A. Danilychev, Yu. M. Popov, and D. D. Khodkevich, Pis'ma Zh. Eksp. Teor. Fiz., 12, 473 (1970).
80. V. Yu. Baranov, V. M. Borisov, Yu. B. Kiryukhin, and Yu. Yu. Stepanov, Kvantovaya Elektron. (Moscow), 5, 2285 (1978).
81. A. Z. Grasyuk, I. G. Zubarev, A. V. Kotov, S. M. Mikhailov, and V. G. Smirnov, Kvantovaya Elektron. (Moscow), 3, 1062 (1976).